Impact Hazard Protection Efficiency by a Small Kinetic Impactor

J.P. Sanchez[1]
University of Strathclyde, Glasgow, Scotland G1 1XH, United Kingdom

C. Colombo[2]
University of Strathclyde, Glasgow, Scotland G1 1XH, United Kingdom

In this paper the ability of a small kinetic impactor spacecraft to mitigate an Earth-threatening asteroid is assessed by means of a novel measure of efficiency. This measure estimates the probability of a space system to deflect a single randomly-generated Earth-impacting object to a safe distance from the Earth. This represents a measure of efficiency that is not biased by the orbital parameters of a test-case object. A vast number of virtual Earth-impacting scenarios are investigated by homogenously distributing in orbital space a grid of 17,518 Earth impacting trajectories. The relative frequency of each trajectory is estimated by means Opik's theory and Bottke's near Earth objects model. A design of the entire mitigation mission is performed and the largest deflected asteroid computed for each impacting trajectory. The minimum detectable asteroid can also be estimated by an asteroid survey model. The results show that current technology would likely suffice against discovered airburst and local damage threats, whereas larger space systems would be necessary to reliably tackle impact hazard from larger threats. For example, it is shown that only 1,000 kg kinetic impactor would suffice to mitigate the impact threat of 27.1% of objects posing similar threat than that posed by Apophis.

Nomenclature

a	=	semi-major axis of an orbit, km
b^*	=	b-plane impact parameter, km
D	=	asteroid's diameter, km or m

[1] jpau.sanchez@strath.ac.uk, Research Fellow, Advanced Space Concepts Laboratory, Department of Mechanical and Aerospace Engineering, University of Strathclyde, Glasgow
[2] c.colombo@soton.ac.uk, Research Fellow, Advanced Space Concepts Laboratory, Department of Mechanical and Aerospace Engineering, University of Strathclyde, Glasgow

$D_{Elowbound}$ = asteroid's diameter yielding minimum energy in an energy event, km or m

$D_{Eupperbound}$ = asteroid's diameter yielding maximum energy in an energy event, km or m

$D_{Maxsize}$ = maximum asteroid's diameter that can be deflected within a $\Delta t_{warning}$, km or m

$D_{Minsize}$ = minimum asteroid's diameter discovered within a Δt_{survey} , km or m

d_{min} = minimum distance, km or AU

E_{impact} = impact energy, MT

e = eccentricity of an orbit

e_{impact} = specific impact energy, J/kg

$f_I(.)$ = asteroid's impact probability

G = phase slope parameter

$g(.)$ = collision probability function

H = asteroid's absolute magnitude

I_{eventD} = impact event cumulative distribution

I_{sp} = specific impulse of a propulsion system, s

i = inclination of an orbit, deg

l = distance between Earth and asteroid when the latter is at its MOID-zero point, km or AU

M = mean anomaly of an orbit, deg

M_{Ast} = mass of the asteroid, kg

$\mathrm{MOID}_{\oplus}$ = critical MOID for which an asteroid would impact Earth

m_d = mass of the spacecraft at impact, kg

$N(.)$ = cumulative number of objects

$P_{col:\mathrm{MOID=0}}$ = probability of collision with Earth of a MOID-zero orbit

p = semilatus rectum of an orbit, km

p_v = asteroid´s albedo

$R_{\oplus}$ = distance between the asteroid and the Earth, AU

$R_{\odot}$ = distance between the asteroid and the Sun, AU

r_a = minimum distance between the Earth and the hyperbola´s asymptote, km

r_p = periapsis distance, km

$r_{\oplus}$ = Earth's radius, 6,378.2 km

ToF = time of flight of the transfer, s

t = time, s or d

t_d = deflection time or time at which impact occurs, s or d

t_{impact} = time at which the asteroid is bound to impact the Earth, s or d

t_{launch} = time at which spacecraft is launched from Earth, s or d

t_{sf} = final time of the asteroid's survey, s or d

t_{si} = initial time of the asteroid's survey, s or d

V = asteroid's apparent magnitude

V_{lim} = limiting visual magnitude

$\mathbf{v}_{Ast}$ = asteroid's orbital velocity vector, km/s

$\mathbf{v}_{\oplus}$ = Earth´s orbital velocity vector, km/s

v_{impact} = asteroid's impact velocity, km/s

v_{∞} = hyperbolic excess velocity of the asteroid, km/s

$\alpha_{\Delta\mathbf{v}_{S/C}}$ = in-plane angle between the $\Delta\mathbf{v}_{S/C}$ and the $\mathbf{v}_{Ast}$, rad or deg

β = momentum enhancement factor

γ = flight path angle, rad

$\Delta\mathbf{v}_{S/C}$ = relative velocity of the spacecraft with respect to the asteroid, m/s or km/s

$\Delta t_{warning}$ = warning time, years

Δt_{survey} = time-length of the survey campaign, years

$\delta\mathbf{r}$ = displacement of the asteroid position at the impact point, km

$\delta\mathbf{v}$ = impulsive change of velocity vector, m/s or km/s

$\delta_{\Delta\mathbf{v}_{S/C}}$ = out-of-plane h direction angle of $\Delta\mathbf{v}_{S/C}$, rad or deg

ε = hyperbolic factor

k = solar phase angle, rad

$\mu_{\odot}$ = gravitational constant of the Sun, $3.9644\text{x}10^{-14}$ AU^3/s^2

$\mu_{\oplus}$ = gravitational constant of the Earth, $3.9860\text{x}10^{5}$ km^3/s^2

$\rho(.)$ = near Earth asteroid density distribution

$\mathbf{\Phi}[.]$ = transition matrix

Ω = argument of the ascending node of an orbit, deg

Ω_{impact} = argument of the ascending node of an impacting trajectory, deg

ω = argument of the perigee of an orbit, deg

ω_{impact} = argument of the perigee of an impacting trajectory, deg

$\omega_{\oplus}$ = Earth´s angular velocity, rad/s

Subscripts

$\oplus$ = relative to the Earth

$\odot$ = relative to the Sun

I. Introduction

Asteroids have long been recognized as both a threat to Earth, as well as an opportunity. As remnants of the formation of our solar system, asteroids and comets provide a precious opportunity to unveil the mysteries of the solar system formation, evolution and composition. On the other hand, Earth is periodically hit by these objects, which permanently alters the characteristics of our planet to varying degrees [1]. Asteroid impacts range from events causing mass extinctions such as the Cretacious-Terciary impact that resulted on the extinction of the dinosaurs [2], to much more modest impacts such as the air blast occurred in 1908 near the Russian Tunguska river [3]. The awareness of the impact risk has led to an intense surveying effort, which now-a-days is responsible for tracking about 9000 Near-Earth Objects (NEOs) [4].

The general recognition that Earth is regularly struck by small objects, together with the increasing number of asteroid discoveries, has also stimulated an intense debate on deflection strategies (see, for example, in the Planetary Defence Conference series[3]). An outcome of this is a growing catalogue of different concepts for asteroid deflection that range from very subtle changes on the optical properties of the asteroid [5] to the much more blunt use of nuclear warheads [6]. In between, other noticeable examples are; low-thrust tugboats [7], gravity-tractors [8], mass drivers [9], solar collectors [10] , ion-beam shepherds [11] and many others. Some of these deflection methods require substantial technological advancements, such as, for example, solar collectors or mass drivers, while others are considered to be at a high technological readiness level (TRL) [12]. Among the latter group, the simplest concept and, probably, highest TRL is the kinetic impactor strategy, which involves changing the asteroid's linear momentum by impacting a spacecraft into it [13, 14].

[3] http://www.planetarydefense.info/

Considerable efforts have also focused on comparing the different asteroid deflection concepts in an attempt to assess the optimal deflection strategy. In a NASA study [15], for example, the preliminary mission design of a comprehensive set of deflection alternatives was performed for a set of five NEO impacting scenarios. The system performance was described by the "effective momentum change" (i.e., Δv required for the deflection multiplied by the NEO's mass) and launch mass. Sanchez et al. [12] performed a multi-objective comparative assessment of six different deflection strategies for thirteen different impact scenarios, characterized by different orbital elements, masses, and physical characteristics of the impacting objects. Also, Schaffer et al. [16] used a multi-objective comparison in order to select the best mitigation option against three notional asteroid impact threats. These, and other, deflection assessments reflect the challenge to define the optimality of a deflection strategy if nothing on the threatening object itself is known, and the necessity of using notional impact scenarios as test cases for the deflection methods.

This paper re-examines the kinetic impactor option while also considering the epistemic uncertainty of the asteroid impact threat. In a previous analysis on the kinetic impactor option, it was shown that with a small spacecraft and very simple transfer strategies, it is possible to obtain considerable deviations for most of the threatening asteroids [17]. In that work, optimal impact trajectories (direct and via a single Venus gravity-assist) to an extract of 30 Potentially Hazardous Asteroids (PHAs) taken from the JPL catalogue of asteroids were designed and analyzed. It has also been shown that, when compared with other more complex deflection alternatives, the kinetic impactor still offers a reasonable option for relatively small objects [12].

Thus, the paper aims to improve the understanding of the capability of a kinetic impactor with current space engineering technology to offer planetary protection from realistic impact threats. A simple figure of merit is used here to convey a good understanding of the capability of a deflection system to provide protection against the general impact hazard. This figure is named thereafter the *Planetary Protection* of the deflection system and provides a quantitative measure of the ability of the deflection system to mitigate any possible Earth-impacting object. This is achieved by estimating the probability of succeeding in deflecting to a safe Earth distance a randomly generated impact threat. A vast number of realistic impact threats are therefore required to be investigated in order to obtain a statistically meaningful sample of deflection scenarios.

A realistic set of impact threat scenarios is built by generating more than 17,000 virtual Earth-impacting trajectories with orbital Keplerian elements homogeneously distributed within the semi-major axis, eccentricity, inclination $\{a,e,i\}$ space of Earth crossing objects. A good estimate of the relative frequency of each of these Earth-impacting orbits can be computed by using the theoretical Near-Earth Object (NEO) distribution by

Bottke et al. [18]. The asteroid's argument of the periapsis ω defines then the Minimum Orbital Intersection Distance (MOID) with the Earth, whereas the mean anomaly M at a given Epoch defines the actual closest encounter. Opik's formulation [19], together with Bottke's Near-Earth Object distribution, is used to estimate the relative impact frequency or probability of a hypothetical threatening object to have a given set of ephemerides.

The mitigation action produced by the kinetic impactor can be well modeled as an instantaneous variation of the velocity of the asteroid at the impact time. The conservation of linear momentum ensures then a linear relation between the mass of the asteroid and the asteroid's variation of velocity. Thus, if the mass of the impacting spacecraft and the impact velocity vector are defined, the size of the largest asteroid that can be deflected by a safe distance from the Earth can also be computed. For each single asteroid's orbit in the set of virtual threatening objects an Earth-to-asteroid interception trajectory is optimized in order to maximize the displacement of the asteroid at the MOID following the kinetic deflection. The deflection achieved at the Earth is computed by an analytical formulation making use of proximal motion equations expressed as a function of orbital elements, which provides a good accuracy and reduces the computational effort [17].

The paper aims to understand the realistic capability to mitigate impact hazard with current space technology. For this reason, a small deflection mission is assumed; a 1,000 kg spacecraft is launched from Earth with 2.5 km/s of escape velocity v_∞. In the view of recent missions to asteroids, such as NASA's Dawn mission [20], ESA's Rosetta mission[4] or Deep Impact [21], this can be considered a perfectly plausible mission with current space technology. Moreover, it is important to consider that in a real impact threat scenario, i.e., when an asteroid is bound to hit the Earth, if a deflection attempt is arranged, higher levels of funding than those seen today for scientific missions should be expected, and thus, a 1-tonne deflection system can here be considered *small*.

For the sake of completeness, two distinct cases are envisaged in this paper. On the first one, we assume that the impact threat is know, thus it has been previously detected and surveyed by an asteroid detection system. This allows us to define the level of planetary protection purely achieved by the kinetic impactor system. On the other hand, this can be put into a wider, and more realistic, context by considering that the impact threat requires to be detected by a survey system prior to any deflection attempt. While the definition of the kinetic deflection system (i.e., 1-tonne and excess velocity at launch of 2.5 km/s) poses a maximum limiting size that can be deflected, the need for the impacting threat to be detected imposes also a minimum object size that can

[4] http://sci.esa.int/science-e/www/area/index.cfm?fareaid=13 [Last retrieved 1 December 2011]

realistically tackle. For each of these two cases, one can then estimate the fraction of impact hazard (over all the possible impact scenarios) that a small kinetic deflection system should be able to mitigate.

The paper is organized as follow: Section II describes the methodology to create a comprehensive list of ephemeris made up with more than 17,000 impacting trajectories. Each impacting orbit is then tagged with its relative impact frequency. Section III gives an account of the method and model used to describe a complete deflection mission. This includes trajectory design through global optimization, the impact model and final deflection calculation. Moreover, a detection model, which attempts to provide a measure of the likelihood of discovery of an object on an Earth-impacting course, is described. As will be shown, the detection model is only a simple account that captures the essentials of the asteroid detection problem and allows us to define the capabilities of a notional asteroid survey. Section IV summarizes the results of the optimized deflection scenarios and the planetary protection achieved by a small kinetic impactor system. Finally, Section V concludes with a brief discussion of the results.

II. Set of impacting orbits

A set of Earth-impacting orbits was created as comprehensive set of impact hazard scenarios to be tackled by a realistically-sized kinetic impactor. In order to provide an assessment of the capabilities of such a system for impact hazard mitigation, i.e., planetary protection, the number of deflection mission analyzed here needs to be much larger than in previous deflection studies [12, 17]. The set of impacting trajectories presented here is made up of 17,518 different ephemeris sets. All of these yield an impact at the same pre-defined epoch. The present section summarizes how the set of impacting orbits was created.

A. Earth impacting orbits

The $\{a,e,i\}$-domain is first divided into a three-dimensional grid containing over 28,000 points homogeneously distributed within a semi-major axis a from 0.05 to 7.35 AU, eccentricity e from 0.025 to 0.975 and inclination i from 0 to 87.5 degrees. Only 8,759 locations in this grid correspond to orbits with a perihelion smaller and aphelion larger than 1 AU (see the grid in Figure 1). The latter is a necessary, but not sufficient, condition for an impact trajectory when an Earth 1 AU circular orbit is considered, as it is here.

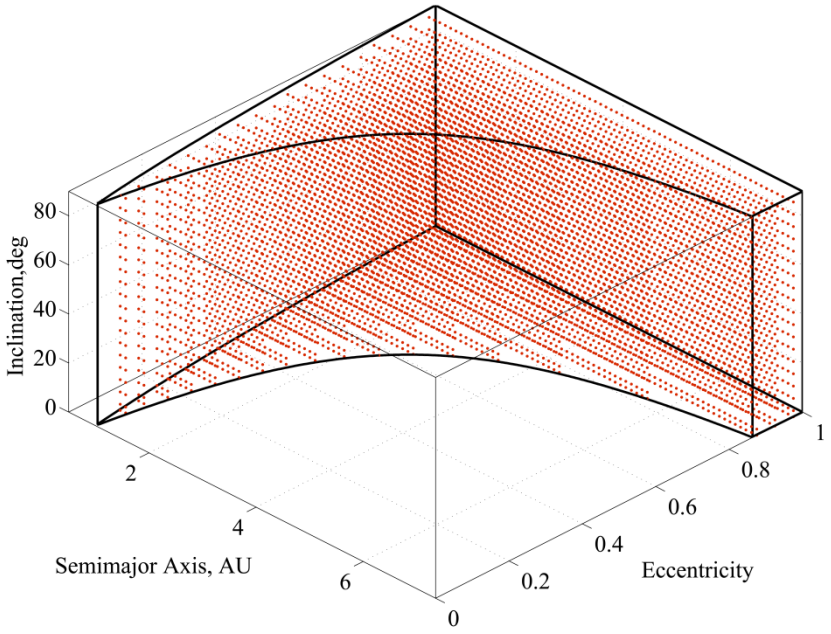

Figure 1: Homogenously distributed grid set of Earth-impacting trajectories.

Under the approximation of a circular orbit for the Earth, it is relatively straightforward to compute also the ascending node Ω_{impact} and the argument of periapsis ω_{impact} that allow an object with a fixed semi-major axis a, eccentricity e, and inclination i to cross the orbit of the Earth at a given angular position. As is shown in Figure 2, Ω_{impact} is uniquely defined by the position of the Earth at the fixed epoch at which the virtual impact is set (see cross symbol in Figure 2, which represents the Earth's location at a given epoch), while ω_{impact} has two possible configurations corresponding to the two thick-dashed orbits in Figure 2. Note that ω_{impact} reported in Figure 2, with the red arc, corresponds to the argument of the orbit with apoapsis below the orbit of the Earth, whereas the opposite orbit would be represented by $-\omega_{\text{impact}}$. Due to these two existing values of ω_{impact}, these 8,759 grid locations define in reality 17,518 different virtual impacting trajectories. This full set of impacting ephemerides will be used here to assess the deflection capability of the kinetic impactor system.

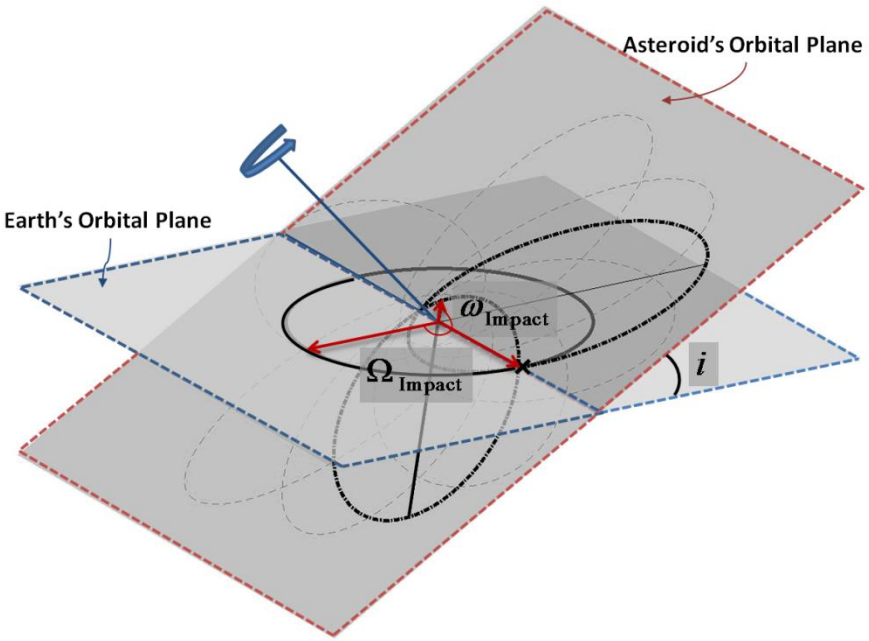

Figure 2: Orbital geometry of possible impactors for a given semi-major axis *a*, eccentricity *e* and inclination *i*.

Another consequence of assuming the Earth is on a 1 AU circular orbit is that the excess velocity v_∞ of any possible encounter can be defined analytically as a function of semi-major axis *a*, eccentricity *e* and inclination *i* of the asteroid by means of Tisserand's criterion:

$$v_\infty = \sqrt{\mu_\odot \left(3 - \frac{1}{a} - 2\sqrt{a\left(1-e^2\right)}\cos i \right)} \tag{1}$$

where $\mu_\odot$ is the gravitational constant of the Sun and both semi-major axis and $\mu_\odot$ need to be expressed in AU units. The final impact velocity can then be computed by accounting for the Earth's gravity as:

$$v_{impact} = \sqrt{\mu_\oplus \left(\frac{2}{r_\oplus} - \frac{v_\infty^2}{\mu_\oplus} \right)} \tag{2}$$

where $r_\oplus$ and $\mu_\oplus$ represent respectively the radius and gravitational constants of the Earth. Note that the specific impact energy, or energy-mass fraction, yielded by each impacting orbit

$$e_{impact} = \frac{E_{impact}}{M_{Ast}} = \frac{1}{2} v_{impact}^2 \tag{3}$$

is also pre-defined, since v_{impact} is an explicit function of the impact trajectory, where M_{Ast} is the mass of the asteroid. Therefore, as will be explained in more detail in a later section, a figure defining the impact protection capability of a given kinetic impactor can be provided by estimating the largest asteroid that could be deflected from a collision trajectory from each of the virtual impactor orbits.

B. Impact probability

As can be seen, for example, in Ref. [18], there are regions of space much more densely populated with near-Earth objects than others. There are, for instance, many more low inclination than high inclination objects. On the other hand, not only the NEO population density is important when considering impact frequency, but also the impact geometry of the orbit plays an important role. Thus, each of the 17,518 homogeneously distributed virtual impactors do not have the same likelihood of existing and this needs to be accounted for when considering levels of planetary protection. The relative frequency of each virtual impactor is therefore assessed individually, by means of two multiplying factors; first, the NEO orbital distribution that defines the actual asteroid probability density, and second, the collision probability of a given set of $\{a,e,i\}$, which assesses the likelihood of impact for a given object.

NEO orbital distribution

The NEO orbital distribution used here is based on an interpolation from the theoretical distribution model published in Bottke et al. [18]. The data used was very kindly provided by W. F. Bottke (personal communication, 2009). An orbital distribution of NEOs was built by propagating in time thousands of test bodies initially located at all the main source regions of asteroids (i.e., the ν6 resonance, intermediate source Mars-crossers, the 3:1 resonance, the outer main belt, and the trans-Neptunian disk). By using the set of asteroids discovered by Spacewatch at that time, the relative importance of the different asteroid (or comets) sources could be best-fitted. This procedure yielded a steady state population of near Earth objects from which an orbital distribution as a function of semi-major axis a, eccentricity e and inclination i can be numerically interpolated. Figure 3 shows a representation of Bottke's NEA density $\rho(a,e,i)$ as a set of grid points colored and sized as a function of the values of the NEO density ρ.

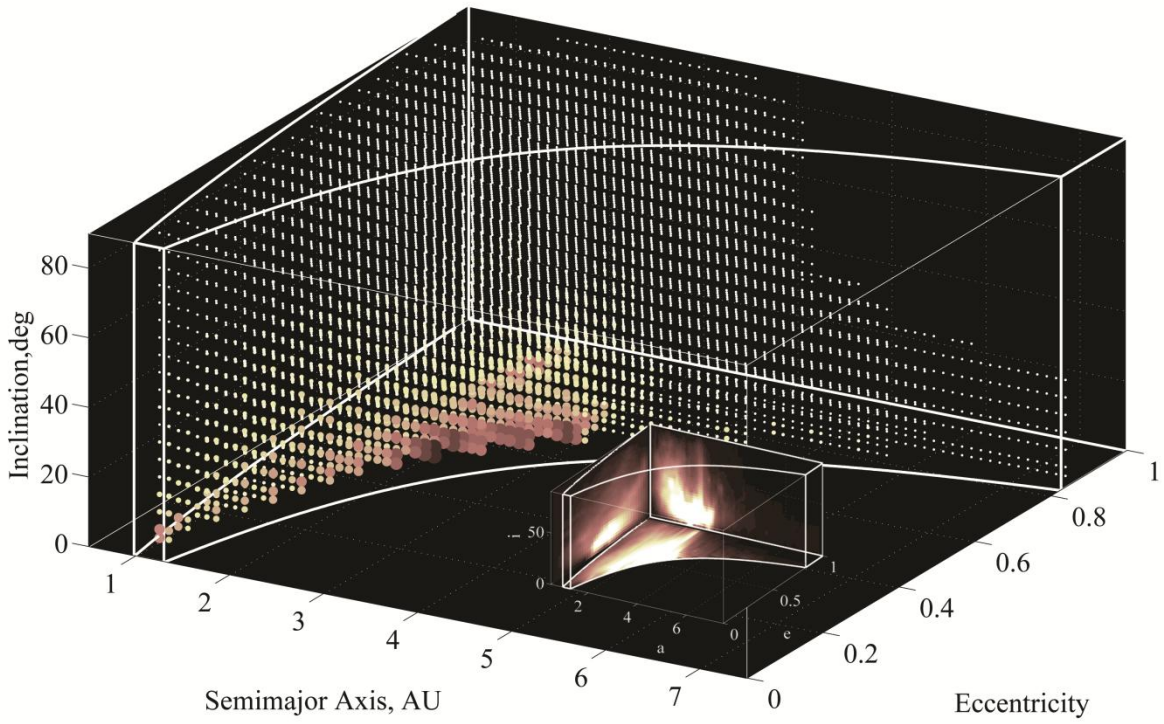

Figure 3: Theoretical Bottke et al. [18] NEO distribution. The figure shows a representation of the NEO density function $\rho(a,e,i)$. The 4th dimension, i.e., the density ρ at a given point (a,e,i), is represented by a set of grid points colored and sized as a function of the value ρ. A smaller set of axes represent the projection of the total value of ρ onto the planes a=0.5 AU, e=1 and i=0 deg. Note that the color code has been inverted for the smaller projection figure to improve clarity.

Probability of collision of an asteroid

A necessary condition for an asteroid to impact the Earth is to have both a perihelion smaller and aphelion larger than 1 AU. This, of course, it is not sufficient, since only a very limited set of arguments of periapsis ω will actually yield a trajectory crossing Earth's orbital path (see Figure 2). For a given epoch, that is a fixed position of the Earth within its orbital path, only a single ascending node Ω allows the asteroid trajectory to intersect the Earth (see Figure 2). Finally, only one possible mean anomaly M allows the asteroid to meet the Earth at the same exact position. Hence, the NEA density distribution $\rho(a,e,i)$, which defines the probability of finding an asteroid with given $\{a,e,i\}$ based on known asteroid population evolution, is not yet a measure of how likely is to find an impactor with a given set of Keplerian elements. The present section will now define the collision probability function $g(a,e,i)$ which describes the relative frequency with which an asteroid with a given $\{a,e,i\}$ should meet the Earth along its trajectory.

The MOID is referred to here as the minimum orbital distance possible between two orbits and, particularly, in the case at hand between the Earth and an asteroid. In order to compute the collision probability of an asteroid with Keplerian elements $\{a,e,i\}$, we first need to compute the maximum MOID that allows an Earth collision. For the latter, the Earth's gravity needs to be accounted, since an asteroid close to Earth will essentially follow a hyperbolic trajectory with the Earth at its focus. A hyperbolic factor ε,

$$\varepsilon = \frac{r_a}{r_p} = \sqrt{1 + \frac{2\mu_\oplus}{r_p v_\infty^2}} \tag{4}$$

accounts then for the curvature that the object's trajectory would experience during the Earth approach. In Eq. (4), r_a is the minimum distance between the hyperbola asymptote and the Earth, r_p is perigee distance of the asteroid's hyperbolic trajectory, $\mu_\oplus$ is the gravitational constant of the Earth and v_∞ the hyperbolic excess velocity of the asteroid as given in Eq. (1). Thus, if we assume that the maximum distance for a collision to occur is one Earth radius $r_\oplus$, the actual maximum geometrical distance between the orbit of the Earth and the asteroid will require to be smaller than

$$\mathrm{MOID}_\oplus = r_\oplus \sqrt{1 + \frac{2\mu_\oplus}{r_\oplus \cdot v_\infty{}^2}} \,. \tag{5}$$

The following sub-section will describe an analytical approximation of the MOID that allows us to easily compute the range of argument of the periapsis ω such that the asteroid's MOID is smaller than $\mathrm{MOID}_\oplus$. Two important assumptions allow us to proceed: firstly, we have already assumed a circular 1 AU orbit for the motion of the Earth, and secondly, we assume that the right ascension of the ascending node Ω and the argument of periapsis ω are uniformly distributed random variables. The ascending node Ω and the argument of periapsis ω are generally believed to be uniformly distributed in near Earth orbit space as a consequence of the fact that the period of the secular evolution of these two angles is expected to be much shorter than the life-span of a near Earth object. Therefore, we can assume that any value of Ω and ω is equally possible for any NEA [18]. Similarly, all values of mean anomaly M are also assumed to be equally possible.

Minimum Orbital Intersection Distance

The exact values of ω_{impact} are relatively easy to find by noting that the true anomaly at the ecliptic plane must be such that the distance to the Sun is 1 AU. Two are the possible values of ω_{impact} for an Earth-crossing asteroid to have a collision with the Earth. While an asteroid with argument of periapsis equal to ω_{impact} will have a MOID equal to zero, for arguments of periapsis close to ω_{impact} the variation of MOID can be linearly

approximated [19]. With the axis shown as in Figure 4, the motion of the Earth and the asteroid can be well described using a linear approximation of the Keplerian velocities of the two objects at the encounter. This defines two straight line trajectories, and thus, the minimum distance between these two linear trajectories can be found. The minimum distance can then be written as an explicit function of Δx, which is defined as the distance between the centre of the coordinates described in Figure 4 and the point at which the asteroid crosses the Earth's orbital plane. This minimum distance Δx can alternatively be described as a linear function of the argument of the periapsis ω. Finally, an expression such as [19]

$$\mathrm{MOID}(\omega) = \frac{\left|\omega_{impact} - \omega\right|}{\sqrt{\left(\frac{1}{\sin i}\right)^2 + \tan^2 \gamma}} \tag{6}$$

yields an approximate value of the MOID distance. The absolute value $|\omega_{\mathrm{impact}} - \omega|$ refers to the minimum absolute difference to the two values of ω_{impact} and the tangent of the flight path γ angle can be calculated as:

$$\tan \gamma = \frac{p}{\sqrt{e^2 - (p-1)^2}} \tag{7}$$

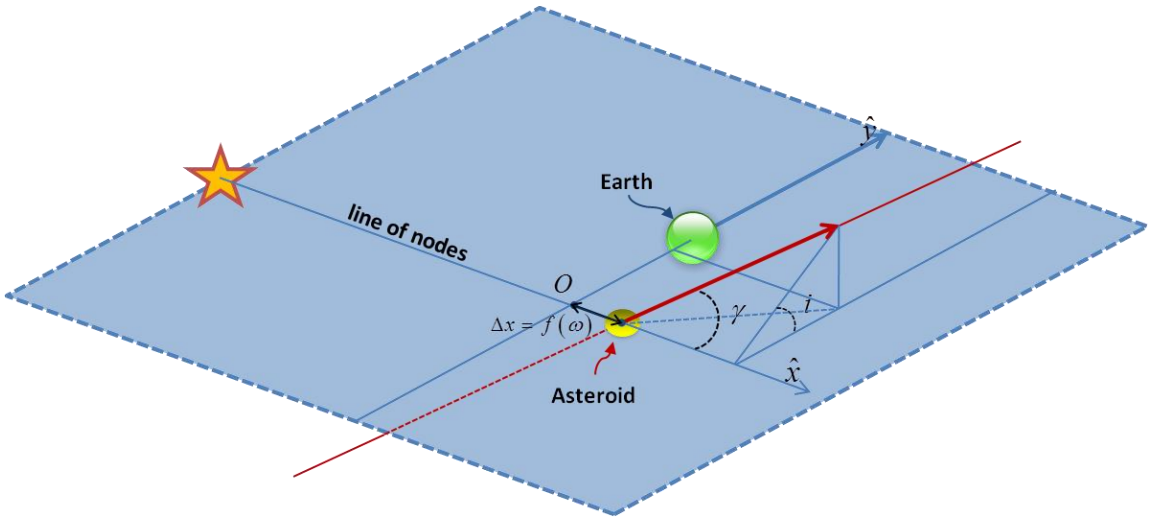

Figure 4: Set of coordinates used to compute Eq. (6).

As can be seen in [22], Eq. (6) provides a good approximation of the numerically calculated MOID even for values not extremely close to ω_{impact}.

Probability of having a MOID lower than the collision distance

Since Eq. (5) defines the maximum MOID at which a collision would occur, by rearranging Eq. (6) it is possible to define the range of argument of periapsis for which an asteroid would have a MOID smaller than $\mathrm{MOID}_{\oplus}$:

$$\Delta\omega = \mathrm{MOID}_{\oplus} \cdot \sqrt{\left(\frac{1}{\sin i}\right)^2 + \tan^2\gamma} \tag{8}$$

Twice the value of Eq. (8) provides the total range of ω that yields a MOID smaller than $\mathrm{MOID}_{\oplus}$ for one of the two impactors in each point of the grid, and since there are there are two different impactors, the total range shall be $4\Delta\omega$. Lastly, since the argument ω has been assumed a uniformly distributed random variable and the total range of possible arguments ω is 2π, the probability of having an argument ω such that the impact can occur is:

$$g\left(a,e,i\right)_{\omega} = \frac{2\cdot\left(2\cdot\Delta\omega\right)}{2\pi} \tag{9}$$

Probability of collision

Equation (9) defines the probability of having an asteroid such that MOID is small enough for a collision to be possible, nevertheless we still require to know the probability of also having the Earth and the asteroid with a phasing such that the collision occurs. This will now be described by defining the function $g\left(a,e,i\right)_{col}$ or probability of collision with Earth of an asteroid with $\mathrm{MOID} \leq \mathrm{MOID}_{\oplus}$.

As is well known, the shortest distance between two linear trajectories must have a direction perpendicular to both of them, and this must also be satified by the Earth and asteroid linear trajectories as described in Figure 4. As depicted now in Figure 5, this condition defines a cylindrical region around the Earth's linear trajectory that must be crossed by any object with a minimum orbital distance smaller than the radius of the cylinder. Since the motion of an asteroid with defined inclination i (and ascending node Ω) will always be confined within its orbital plane, an elliptical section can be defined as a result of the intersection between the cylinder of radius r and the asteroid's orbital plane (see Figure 5). Note that since the Earth is assumed to be on a circular orbit, the right ascension of the ascending node Ω is actually irrelevant for the calculation of the impact probability. The trajectories of both objects are assumed to be straight lines. An asteroid with a MOID smaller than $\mathrm{MOID}_{\oplus}$ requires crossing the elliptical intersection between the cylinder of radius $\mathrm{MOID}_{\oplus}$ and the asteroid's orbital plane.

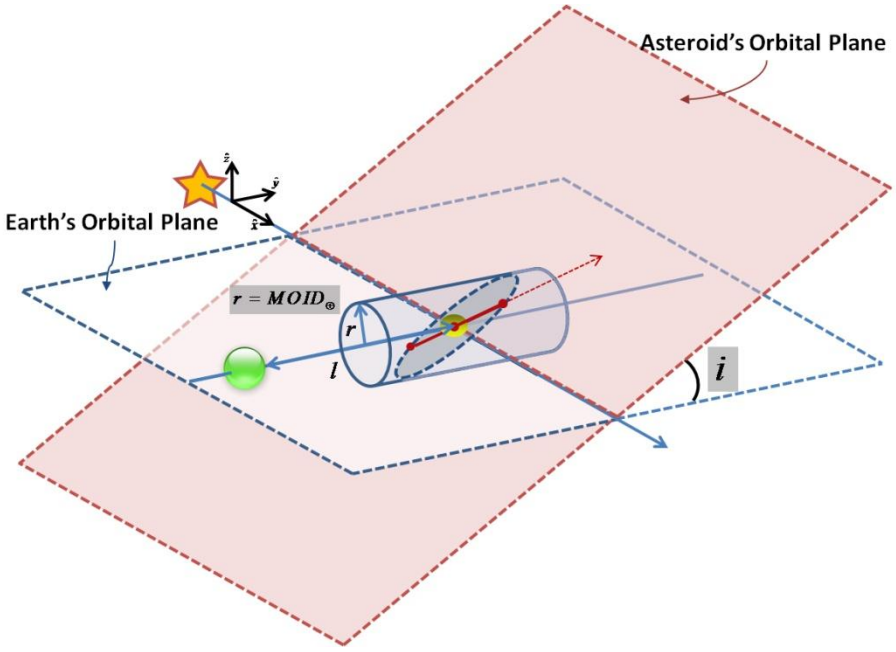

Figure 5: Representation of the Earth and asteroid impact geometry.

Thus, as defined in Figure 5, a necessary, but not yet sufficient, condition for an asteroid to encounter the Earth at distance smaller than r is that its trajectory must intersect the elliptical section drawn by the intersection of a cylinder of radius r and the asteroid's orbital plane. For the case of a cylinder of radius equal to $\mathrm{MOID}_{\oplus}$, only asteroids with arguments of periapsis within $\omega_{\mathrm{impact}} \pm \Delta\omega$ will have trajectories intersecting its elliptical section. Each of these trajectories (i.e., with varying ω within the range $\omega_{\mathrm{impact}} \pm \Delta\omega$) will follow parallel paths, due to the linearly approximated motion, intersecting the elliptical section for a different length, as shown in Figure 6. Aa a consequence, all trajectories would draw parallel chords in the elliptical section. Among all possible trajectories, the central passage yields the trajectory with the longest path within a distance smaller than $\mathrm{MOID}_{\oplus}$. The ellipse's central trajectory corresponds to the orbit with MOID equal to zero. The collision probability of each particular trajectory can then be assumed to be proportional to the path length within the elliptical section.

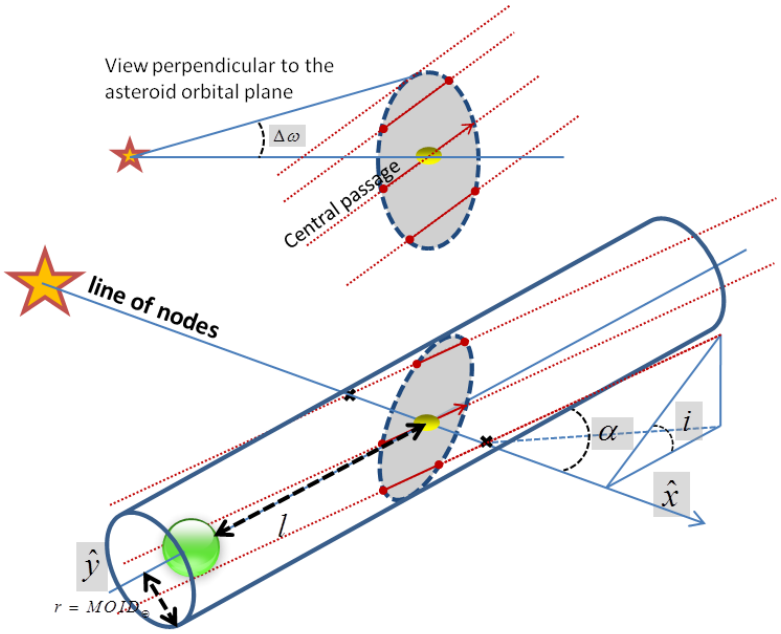

Figure 6: Configuration of asteroid impacting trajectories.

These intersecting trajectories can also be seen as a set of parallel chords of the elliptical section. Then, the average length of the set of parallel chords (or parallel trajectories) crossing an ellipse can be computed to be $\pi/4$ times the length of the central chord/trajectory (i.e., trajectory crossing the centre of the ellipse). Similarly then, the average probability of collision for asteroids with periapsis argument within the range $\omega_{\text{impact}} \pm \Delta\omega$ is assumed to be $\pi/4$ times the probability of collision of the central trajectory:

$$g(a,e,i)_{col} = \frac{\pi}{4} \cdot P(a,e,i)_{col:\text{MOID}=0} \tag{10}$$

where $P_{col:\text{MOID}=0}$ refers to the probability of collision with the Earth of the asteroid trajectory with MOID equal to zero (MOID-zero object), or the central passage of the ellipse pictured in Figure 5 and Figure 6.

In order to compute $P_{col:\text{MOID}=0}$, let us imagine the asteroid at the centre of the ellipse, or point of MOID equal to zero, while the Earth is at a distance l from the same point (see Figure 6). The relative motion of these two bodies in radial-transversal-out-of-plane Cartesian coordinates and using AU as unit length is given by:

$$\left(\sqrt{\frac{\mu_\odot}{p}\left(e^2 - (p-1)^2\right)}, \sqrt{\mu_\odot p} \cdot \cos i - \omega_\oplus, \sqrt{\mu_\odot p} \cdot \sin i \right) \tag{11}$$

where the Earth angular velocity $\omega_\oplus$ is equal to $\sqrt{\mu_\odot}$. Note also that Eq. (1) can be derived from Eq. (11). Using Eq. (11), the minimum distance between the two objects can be calculated:

$$d_{\min} = \sqrt{l^2 \left(1 - \frac{\mu_{\odot} \left(\sqrt{p} \cdot \cos i - 1 \right)^2}{v_{\infty}^2} \right)} \tag{12}$$

If we then set the minimum distance $d_{\min}$ equal to the maximum MOID required for a collision, $\mathrm{MOID}_{\oplus}$, and isolate the variable l, we then obtain the range of positions for which the Earth would actually be impacted by a MOID-zero object at the MOID point:

$$l_{\max} = \frac{\mathrm{MOID}_{\oplus} \cdot v_{\infty}}{\sqrt{\left(v_{\infty}^2 - \mu_{\odot} \left(\sqrt{p} \cdot \cos i - 1 \right)^2 \right)}} . \tag{13}$$

Finally, $P_{col:MOID=0}$ can be easily computed by dividing the total length of possible Earth configurations allowing it to impact the MOID-zero asteroid, i.e., $2l_{max}$, by the total Earth path length in AU units, i.e., 2π.

Collecting the previous subsections, the collision probability of an asteroid is then given by:

$$g(a,e,i) = g_{\omega} \times g_{col} = \frac{l_{\max} \cdot \Delta\omega}{2\pi} . \tag{14}$$

Note that for very low inclinations or very small eccentricities, both $\Delta\omega$ and $l_{\max}$ tend to infinity, and thus, the linear approximation ceases to be valid. To avoid this problem the upper bound of $\Delta\omega$ is set to $\pi/2$, while a numerical search of $l_{\max}$ is performed when the linearly approximated $l_{\max}$ becomes larger than 0.0175 radians (i.e., 1 deg). Similarly to the linear approximation, the numerical search finds the range of the Earth's mean anomaly $\Delta M_{\max}$ for which the minimum distance to a MOID-zero asteroid is equal to $\mathrm{MOID}_{\oplus}$.

Relative frequency of impactors

The set of impactors can finally be weighted with their relative frequency in order to distinguish which regions of the Keplerian element space actually yield a higher impact risk. To compute the relative frequency, the impact probability $f_I(a,e,i) = \rho \cdot g$, where ρ is the NEO density distribution and g the collisional probability, is integrated along the $\Delta a \times \Delta e \times \Delta i$ box centred at each point of the grid, where Δa, Δe, Δi are the grid-mesh step-sizes. Figure 7 shows the complete grid of virtual Earth-impacting objects where each individual point has been colored and sized accordingly to relative frequency that should be expected for each impactor. Four different dot-types have been used in Figure 7 to represent relative impact frequencies as follow: ● <P>≈1%, ● <P>≈0.3%, ● <P>≈0.07% and the smallest refers to <P> <0.01%.

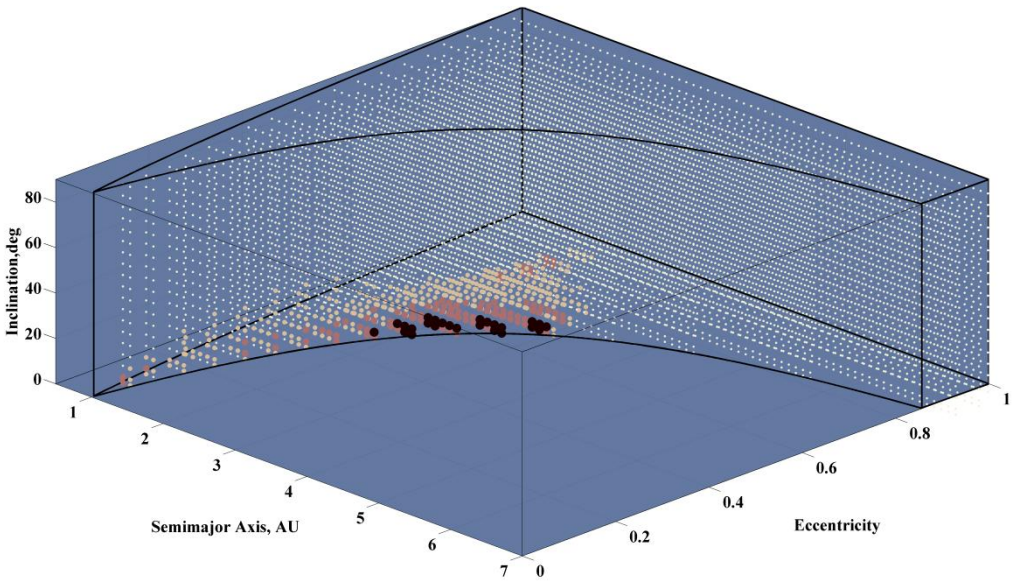

Figure 7: Set of virtual impactors plotted as dots of size and color as a function of the relative frequency that should be expected for each impactor.

III. Deflection scenarios and models

Once the set of Earth-impacting ephemeris has been defined, a deflection mission can be designed by modeling the transfer phase from the Earth to the asteroid interception and the following deflection phase. Then, the maximum deflection achievable for each single impacting ephemeris in the set is computed. As stated earlier, the purpose of the paper is to investigate the ability to provide planetary protection with existing space capabilities. It was therefore chosen here to analyze a kinetic impact system, which can be argued to be the simplest deflection option; other mitigation strategies may be considered in a further work.

A. Kinetic impact deflection

A kinetic impactor mission, with a 1,000 kg wet mass spacecraft and specific impulse $I_{sp} = 300$ s is launched from Earth with 2.5 km/s hyperbolic excess velocity at a given time t_{launch}, previous to the time at which the asteroid is bound to impact Earth t_{impact}. The Earth to asteroid transfer is modeled as direct Lambert's arc with less than one revolution around the Sun. The kinetic impactor spacecraft intercepts and hits the asteroid at a certain deflection time $t_d = t_{\text{launch}} + ToF$, where ToF is the time of flight of the transfer. The impact between the spacecraft and the asteroid is considered to be perfectly inelastic, such that the variation of orbital velocity $\delta\mathbf{v}(t_d)$ of the asteroid imparted by the kinetic impact with the projective spacecraft is given by

$$\delta \mathbf{v}(t_d) = \beta \frac{m_d}{(M_{Ast} + m_d)} \Delta \mathbf{v}_{S/C}(t_d) \tag{15}$$

where the relative velocity $\Delta \mathbf{v}_{S/C}(t_d)$ of the spacecraft with respect to the asteroid at the deflection point is computed from the ephemerides of the asteroid at the deflection time t_d and from the solution of Lambert's arc trajectory. The parameter β represents the momentum enhancement factor, which takes into account effects due to the ejection of mass or gasses, and was set to a conservative value of 1. The mass of the spacecraft at the impact with the asteroid m_d is computed from the rocket equation, subtracting the propellant mass used during the transfer, and M_{Ast} is the mass of the asteroid.

The displacement of the asteroid position at the encounter $\delta \mathbf{r}(t_{\text{impact}})$ following the deflection maneuver Eq. (15) is computed through an analytical formulation derived by Vasile and Colombo [17]:

$$\delta \mathbf{r}(t_{\text{impact}}) \approx \mathbf{\Phi}[t_{\text{impact}}, t_d] \delta \mathbf{v}(t_d) \tag{16}$$

where $\mathbf{\Phi}[t_{impact}, t_d]$ is the transition matrix defined through the proximal motion equations and Gauss's planetary equations. The deflection $\delta \mathbf{r}(t_{\text{impact}})$ is then translated into the impact parameter b^* on the *b*-plane [19], which describes the minimum intersection distance between the deflected asteroid and the Earth, through a matrix rotation described in [17]. Furthermore, the effect of the Earth's gravity on the deflected trajectory of the asteroid is taken into account by including the hyperbolic factor:

$$r_p = \sqrt{\frac{\mu_\oplus^2}{v_\infty^4} + b^{*2}} - \frac{\mu_\oplus}{v_\infty^2} \tag{17}$$

where $v_\infty = (\mathbf{v}_{Ast} - \mathbf{v}_\oplus)$ is the relative velocity of the asteroid with respect to the Earth as given in Eq. (1). Note that Eq. (17) can be rearranged to obtain Eq. (5) if the perigee of the hyperbolic trajectory under the Earth's gravity is set equal to $r_\oplus$.

Through the analytical formulation in Eq. (16) it was possible to define the optimal direction of the deflection maneuver $\delta \mathbf{v}(t_d)$ in order to maximize the magnitude of the deflection r_p for a given time-to-impact $t_{impact} - t_d$ as analyzed in [17]. However, when the transfer trajectory is integrated into the mission design, the ideal optimal deflection conditions cannot always be achieved as also the mass of the spacecraft at the asteroid interception m_d needs to be maximized.

B. Mission design

A global optimization procedure is used to select the optimal transfer conditions to deflect each virtual threatening object on the orbital elements grid by maximizing Eq. (17). Being the impact time defined, the design parameters of the mission are the launch date t_{launch} and transfer time ToF, which, by defining the Lambert's arc trajectory, also specify the impact conditions (i.e., $\Delta\mathbf{v}_{S/C}(t_d)$ and m_d) in Eq. (15) and, thus, the deflection achieved at the Earth's encounter. A global optimization method is used that blends a stochastic search with an automatic solution space decomposition technique. This method has proven to be particularly effective when compared to common optimization methods, especially when applied to space trajectory optimization problems [23, 24]. The time of flight of the transfer trajectory can be chosen within a range $[0.01\ 1.1]T$ where T indicates the greater value between the period of the asteroid and the period of the Earth's orbit around the Sun. Setting the impact date t_{impact} and a warning time $\Delta t_{\text{warning}}$, the launch date can be chosen within the range:

$$t_{\text{launch}} = t_{\text{impact}} - \Delta t_{\text{warning}} + \left(\Delta t_{\text{warning}} - ToF\right)\cdot[0\ 0.99] \tag{18}$$

such that the time-to-impact $t_{\text{impact}} - t_d$ can span from $\Delta t_{\text{warning}} - ToF$ down to $\left(\Delta t_{\text{warning}} - ToF\right)0.01$. The warning time $\Delta t_{\text{warning}}$ is then a paramount parameter of the impact scenario, since it defines the length of the time window within which both transfer and deflection require to be performed. In order to better scan the extended warning time window, two global optimizations are performed; in the first one the search domain can be divided by the optimizer into a sub-domain along the launch time direction down to a depth of branching equal to two. In this way particular regions of the warning time window can be better investigated. Afterwards a subsequent optimization procedure is done, starting with the optimal population of the first run, where the whole domain is explored without any subdivisions [23, 24].

The optimization procedure defines the optimal departure and transfer conditions to maximize the asteroid deflection at the Earth's encounter; in particular this defines the direction of the impacting maneuver on the asteroid. In order to show the influence of the asteroids' orbital elements on the deflection strategy, Figure 9 shows the direction of the deflecting maneuver relative to asteroid's nominal orbit, specifically measured in local tangential-normal-*h* reference frame centered at asteroid at the point of interception by the kinetic impactor spacecraft. We define $\alpha_{\Delta\mathbf{v}_{S/C}}$ as the magnitude of the angle between the projection of $\Delta\mathbf{v}_{S/C}(t_d)$ on the orbital plane of the asteroid $\Delta\mathbf{v}_{S/C}(t_d)\big|_{plane}$ and the direction of motion of the asteroid itself at the time of interception

by the kinetic impactor spacecraft. Analogously, $\delta_{\Delta \mathbf{v}_{S/C}}$ is here defined to be the magnitude of the angle between $\Delta \mathbf{v}_{S/C}(t_d)$ and $\Delta \mathbf{v}_{S/C}(t_d)\big|_{plane}$. Figure 8 shows the angles $\alpha_{\Delta \mathbf{v}_{S/C}}$ and $\delta_{\Delta \mathbf{v}_{S/C}}$.

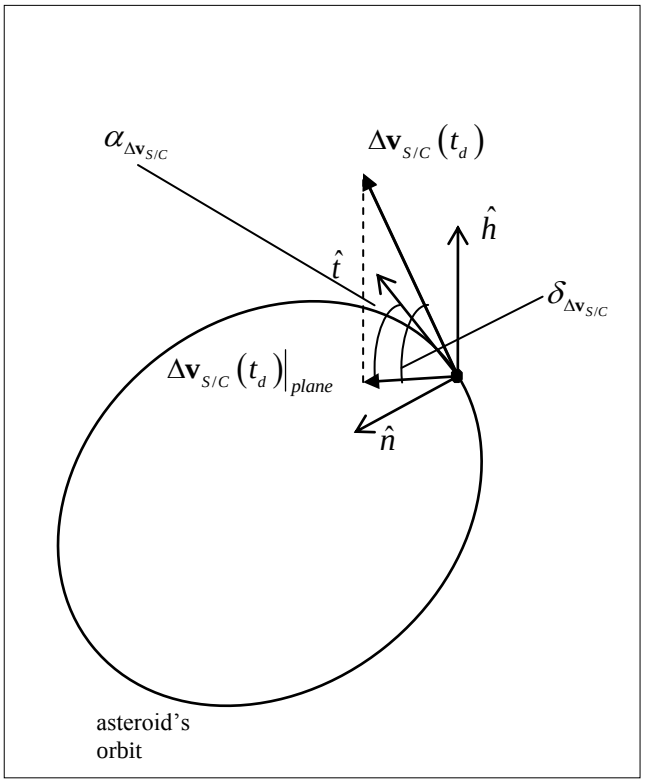

Figure 8: Geometry of the deflection.

The angle $\alpha_{\Delta \mathbf{v}_{S/C}}$, used as color scale in Figure 9a, indicates how far the component of the deflecting action is on the asteroid plane from the tangential direction. It can be noted that for low-inclination asteroids the relative velocity of the spacecraft with respect to the asteroid has a non-zero component along the normal direction in the asteroid orbit plane; for highly inclined asteroids, instead, the velocity of the impacting spacecraft is almost perpendicular to the asteroid nominal orbit plane, as the asteroid is intercepted very close to the ascending node. As a consequence, the relative velocity, has only some component in the out-of plane *h* direction and in the tangential direction, but no component in the normal direction. Moreover it can be asserted that most of the deflection scenarios have the spacecraft breaking the asteroid (the dot symbol in Figure 9a indicates a negative component of $\Delta \mathbf{v}_{S/C}(t_d)\big|_{plane}$ along the tangential direction) and in only few of the scenarios the spacecraft is accelerating the asteroid (the cross symbol in Figure 9a indicates a positive component of $\Delta \mathbf{v}_{S/C}(t_d)\big|_{plane}$ along the tangential direction).

Analogously, in Figure 9b each point of the grid is colored according to angle $\delta_{\Delta \mathbf{v}_{S/C}}$ which gives an indication on how much the deflection maneuver is out of the orbital plane of the asteroid. Moreover the cross or dot symbols in Figure 9b indicate whether the *h*-component of the maneuver is in the *–h* or *+h* direction, respectively. These results are in agreement with the results in Vasile and Colombo [17] although the deflection trajectories are here computed on a much larger set of asteroids, with a wider range of orbital elements. Future work will show a deeper analysis of the deflection trajectories; this is not in our purpose here, hence we limited to discuss the general trend of the deflection trajectory with the asteroid's orbital elements.

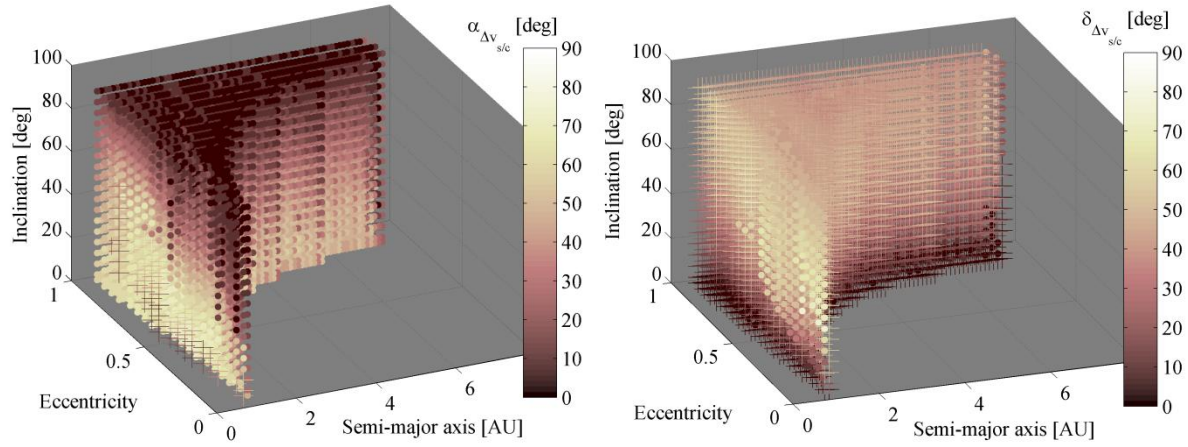

a) **b)**

Figure 9: direction of the deflection maneuver. a) In-plane angle $\alpha_{\Delta v\ s/c}$ of the deflection maneuver; and b) out-of-plane angle $\delta_{\Delta v\ s/c}$.

The analysis of the theoretical optimal direction of the deflection maneuver $\delta \mathbf{v}(t_d)$ performed in [17] identified that a maximum deflection can be achieved if the asteroid is impacted at its perigee, where its orbital velocity is higher, rather than at its apogee, where the orbital velocity is slower. However, when the transfer trajectory is integrated into the mission, the asteroid cannot be always intercepted with the theoretical optimal conditions. Due to their orbital shape with respect to the Earth's orbit, shallow-crosser asteroids, i.e., asteroids with one of their orbital apses not far from 1 AU, with a<1 AU are intercepted at their apoapsis, whereas shallow-crossers with a>1 AU are intercepted at their periapsis. This can be asserted from Figure 10 in which the color scale for the grid represents the angular distance of the interception point from the asteroid perigee. Note that shallow-crossers are represented by nodes in the grid at the outer shell of the *V*-shape, while interior nodes would correspond to deep-crosser asteroids. It can also be noted in Figure 10 that the spacecraft's

interception point moves from the asteroid's apoapsis to the periapsis when the semi-major axis is increased from its minimum to its maximum value at a constant eccentricity.

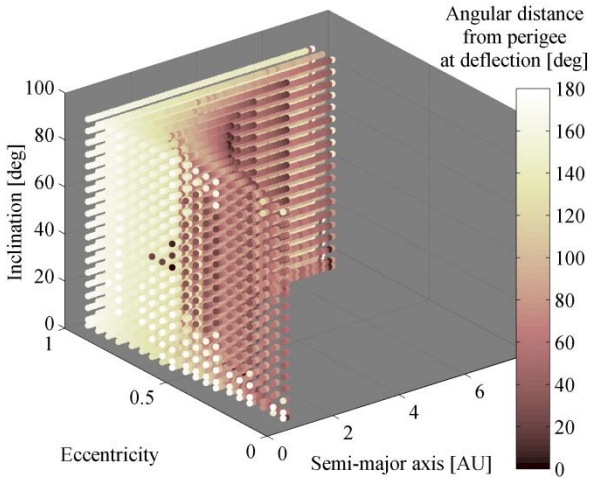

Figure 10: True anomaly of the asteroid interception.

Finally, the performance of the deflection phase are represented in Figure 11 in terms of $\|\delta\mathbf{v}(t_d)\|$ imparted to the threatening body of 10^{10} kg at the deflection position (see color scale in Figure 11a) and the achievable deflection with a 1,000 kg impacting spacecraft and a 20 year warning time available for the overall mission (see color scale in Figure 11b).

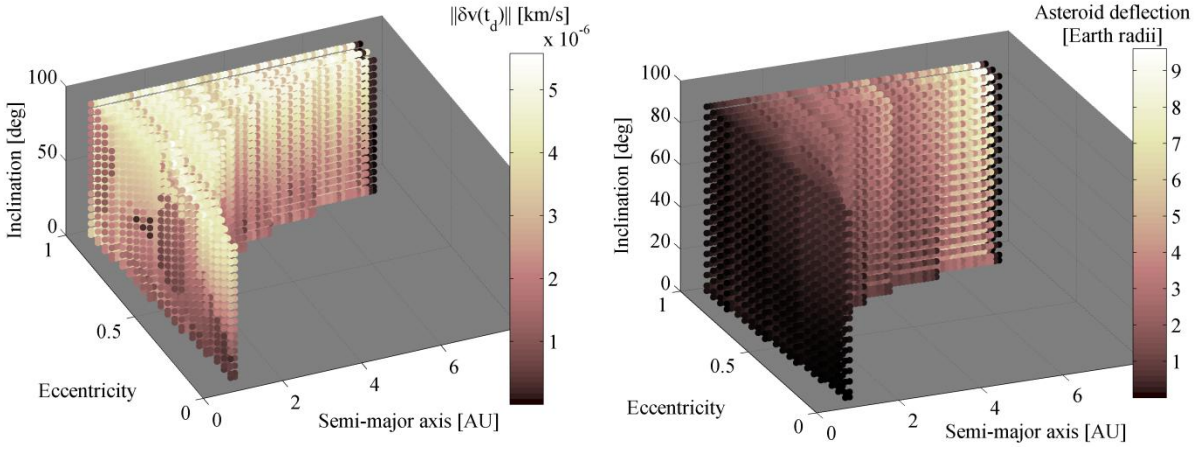

a) **b)**

Figure 11: Asteroid (mass 10^{10} kg) deflection phase for a 1,000 kg impacting spacecraft: a) $\delta v(t_d)$ given to the asteroid at the deflection point and b) deflection in Earth radii (20 years warning time).

C. Impact scenarios

The paper has considered so far that the threatening object is known, that is it has been previously detected and surveyed, and so the kinetic impactor can be deployed as soon as is ready to be launched. For such a scenario, the warning time $\Delta t_{\text{warning}}$ defines then the length of time available to deflect the impacting threat and so it can be varied and analyzed in order to understand how the deflection system copes with scenarios requiring a prompt or a more timely deflection. While this scenario is interesting to understand the deflection capabilities of a kinetic impactor on different type of impacting trajectories and warning times, a more realistic impact hazard scenario should also be considered to assess the difficulty of discovering objects of different size and orbital characteristics. Thus, if a threatening object is on an orbit from which it can be efficiently deflected, it could well happen that this advantage is somehow cancelled by the fact that objects on this orbit approach the Earth very rarely and thus discovery becomes difficult. This paper therefore envisages two different impact scenarios. A first scenario where the virtual threatening object is known, and thus the deflection system can be launch as soon as it is ready (this being defined by the warning time $\Delta t_{\text{warning}}$); and a second case where the threatening object requires first to be detected. For the latter case, a simple asteroid detection model is implemented to compute the smallest detectable object from each point on the grid of virtual impactors as a function of the time-length of the surveying campaign Δt_{survey}. Note that while the optimal design of the kinetic deflection mission defines the maximum object size that can be deflected from each point in the grid of impacting ephemeris, the detection model will now also define a minimum object size that can be deflected, simply because below this size the asteroid cannot be detected and hits the Earth without advance warning.

Asteroid detection model

It is out of the scope of the paper to provide a comprehensive detection analysis of the Earth-impacting asteroids, as, for example, can be found in [25]. Instead, a detection model able to capture the most essential characteristics of a detection of an Earth-impacting object should suffice to put into a wider context the results on the planetary protection achieved by a kinetic impact deflection system. Hence, the detection model proposed here is primarily based on the apparent magnitude V of the asteroid, which can be derived by using [26]:

$$V = H + 5\log_{10}\left(R_{\oplus}\cdot R_{\odot}\right) - 2.5\log_{10}\left(\left(1-G\right)\Phi_1\left(\kappa\right) + G\Phi_2\left(\kappa\right)\right) \tag{19}$$

where

$$\Phi_1\left(\kappa\right) = \exp\left(-3.33\left(\tan\left(\frac{\kappa}{2}\right)\right)^{0.63}\right) \tag{20}$$

$$\Phi_2(\kappa) = \exp\left(-1.87\left(\tan\left(\frac{\kappa}{2}\right)\right)^{1.22}\right) \tag{21}$$

where H is the asteroid's absolute magnitude, $R_\oplus$ and $R_\odot$ are the distances in astronomical units from the asteroid to the Earth and to the Sun, respectively, κ is the solar phase angle and G is the phase slope parameter, which describes how the asteroid brightness falls with increasing solar phase angle. The phase slope parameter G has generally a value between 0 and 1, usually decreasing with decreasing albedo of the asteroid. A constant G parameter equal to 0.15 is assumed here [27].

Equation (19) gives the variation of the visual magnitude with time, as the Earth and asteroid move around the Sun. If we then assume a limiting visual magnitude V_{lim} below which asteroids can be detected, a measure of the smallest asteroid size that can be detected from a given orbit as a function of time can be obtained by;

$$\begin{aligned} D_{smallest}(t) &= \frac{1}{\sqrt{p_v}} \cdot 1329[\text{km}] \times 10^{c/5} \\ c &= -V_{\text{lim}} + 5\log_{10}\left(R_\oplus(t) \cdot R_\odot(t)\right) - 2.5\log_{10}\left((1-G)\Phi_1(\kappa(t)) + G\Phi_2(\kappa(t))\right) \end{aligned} \tag{22}$$

where p_v is the asteroid's albedo, assumed here to be 0.154 as an average value for any asteroid [28]. The limiting visual magnitude V_{lim} is taken as 22.7, which corresponds to the expected capability of the next generation of all-sky surveys (e.g., Pan-STARRS [25]).

In order for a threatening asteroid to be discovered, as defined by the limiting magnitude V_{lim} and Eq. (22), a detection system must be covering the particular area of the sky where the asteroid is found. Ground-based telescopes can obviously search for asteroids only during the night time, and thus only half of the sky is covered by such a system. On the other hand, space-based survey systems allow surveying a larger portion of the sky, although they still have an exclusion zone, of approximately 40 degrees from the Sun direction, that needs to be avoided in order to prevent a low signal to noise ratio due to background sunlight [29]. The paper assumes that multiple ground and space-base surveys are available at any time, and that all the sky is surveyed, except the solar exclusion zone, in a sufficiently small time so that a detection opportunity is not missed. This, of course, is an idealized scenario of the survey capability, but nevertheless an interesting case to be included. Figure 12 provides an overview of the asteroid detection capability, by means of detectable asteroid size in an Earth-Sun rotating system, of a system capable to cover 3.5 steradians of sky and at a limiting magnitude of 22.7. As shown by the figure, small objects, of order a few tens of meters, require a very specific configuration with respect the Earth and Sun in order to be discovered; whereas larger ones, of order a few hundred meters

diameter, are more easily detected. Figure 12 is represented in a synodic reference frame with the Earth and the Sun at 1 AU distance. The Earth is at the centre of the frame.

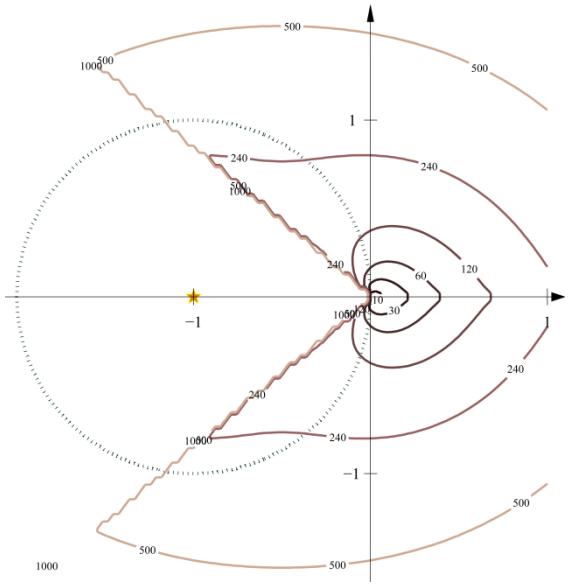

Figure 12: Contour lines for asteroid size detection threshold (in meters) relative to the Sun and Earth position.

As indicated by Eq. (22), $D_{smallest}$ varies as a function of time, hence the minimum asteroid size detectable is the minimum value of $D_{smallest}(t)$ within a given range of time $[t_{si}, t_{sf}]$, where t_{si} is the starting time of the survey, t_{sf} the final time of the survey, and thus, t_{sf}-$t_{si}\equiv\Delta t_{\text{survey}}$ is the duration of the survey campaign. We assume in this paper that no threatening object is detected 25 years prior to impact, therefore the starting time t_{si} for the impact scenario requiring detection is fixed at $t_{si}=t_{\text{impact}}-25$ years. For a given deflection scenario with a fixed warning time $\Delta t_{\text{warning}}$, the final time of the survey is then equal to $t_{sf}=t_{\text{impact}}-\Delta t_{\text{warning}}$. The deflection system is therefore used to deflect any object larger than the minimum discovered size for a survey ranging within $[t_{\text{impact}}-25$ years, $t_{\text{impact}}-\Delta t_{\text{warning}}]$, thus a survey campaign lasting for $\Delta t_{\text{survey}}=25-\Delta t_{\text{warning}}$ [years]. For example, in this paper and in the case of requiring detection prior to a deflection attempt, a mission launched with a warning time of 5 years prior to impact would be used to attempt a deflection to any object larger than the $\min(D_{smallest}(t))$ within the range $[t_{\text{impact}}-25$ $t_{\text{impact}}-5]$, thus a 20-years long survey. Figure 13 shows the distribution of minimum asteroid size discovered for such a notional survey as a function of Keplerian elements.

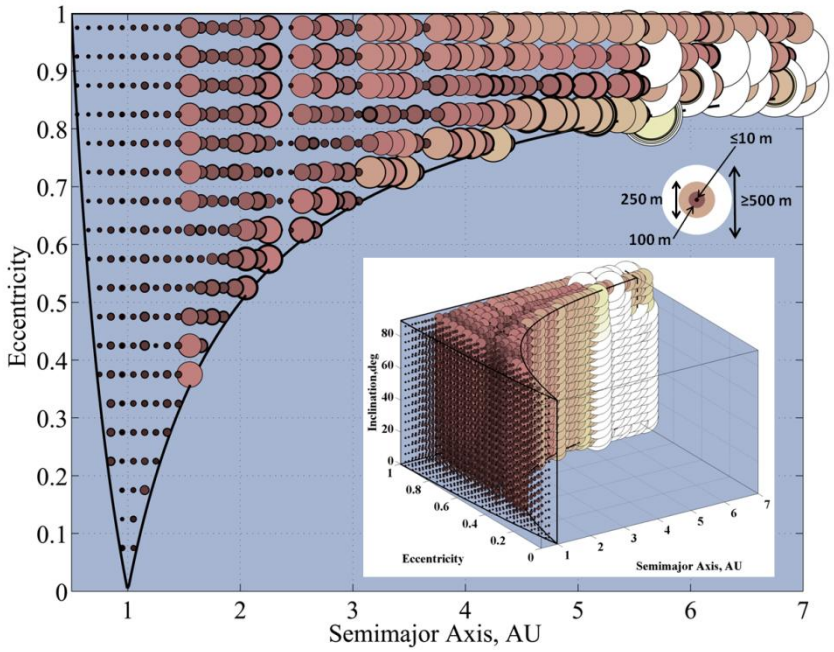

Figure 13: $D_{smallest}$ for a survey time span of 20 years starting at t_{impact}-25 years.

Figure 13 reveals some interesting features for the discovery of Earth impacting objects. We must first note that all the objects analyzed in Figure 13 have a preset Earth impact trajectory, thus at some date t_{impact} all these trajectories intersect the Earth. In general, an asteroid is more prone to be discovered when passing through its MOID point. Hence, in this case, through the orbital position that at t_{impact} yields an impact with the Earth (i.e., MOID zero point). A small semi-major axis is equivalent to a short period, and thus within 20 years of survey the asteroid experiences many more MOID passages. As expected then Figure 13 shows smaller asteroids for semi-major axis close to 1 AU. For large semi-major axis, the asteroid may experience very few passages through sections of its orbit close to the Earth's orbital path (i.e., at 2 AU the asteroid will experience 7 passages, while at 5 AU only 1) and thus discovery opportunities are more scarce. Some quasi-resonances can also be seen in Figure 13 that allows threatening objects to be easily spotted despite the scarcity of the MOID passages; this can for example be observed at 2.35 AU. We can also note that shallow-crossers tend to be slightly more difficult to detect than objects crossing the orbit of the Earth more deeply (i.e., higher eccentricity). Finally, the asteroid's inclination seems to affect in little to the discovery opportunities and likelihood, except for rare cases in which asteroid is discovered behind the Sun. For these cases, a high inclination allows the asteroid to exit the survey exclusion zone while still moving relatively close to the pericenter.

Planetary protection

The *planetary protection* can be defined as the probability of a deflection system to deflect a random impact threat. Since this figure is computed by analyzing the efficiency of the deflection system over a very large set of impact ephemeris homogenously distributed over all possible impact geometries, it is argued here that the planetary protection provides a quantitative measure of the efficiency of an impact deflection system that is not biased by the orbital elements of a particular asteroid. This section will now discuss the level of planetary protection, and thus the mitigation efficiency, provided by a kinetic impactor system, and in particular by a small 1-tonne spacecraft launch from Earth with an excess velocity of 2.5 km/s.

We first define the seriousness of an impact threat, which can be done by means of a sole parameter; the impact energy. By following, approximately, the definitions proposed in [4], the impact hazard can be divided into six categories defined by their range of impact energy, as described in Table 1.

Table 1. Impact hazard categories.

Type of event	Approximate range of impact energies (MT)	Approximate range size of impactor	Relative event frequency
Airburst	1 to 10 MT	15 to 75 m	~177,000 of 200,000
Local Scale	10 to 100 MT	30 to 170 m	~20,000 of 200,000
Regional Scale	100 to 1,000 MT	70 to 360 m	~2400 of 200,000
Continental Scale	1,000 MT to 20,000 MT	150 m to 1 km	~600 of 200,000
Global	20,000 MT to 10,000,000 MT	400 m to 8 km	~100 of 200,000
Mass Extinction	Above 10,000,000 MT	>3.5 km	~1 of 200,000

The impact energy E_{impact} is defined by the mass and impact velocity of the threatening object as:

$$E_{impact} = \frac{1}{2} M_{Ast} v_{impact}^2 \,. \tag{23}$$

The impact velocity v_{impact} of each impactor in the grid is defined as described in section II (i.e., Eq. (1) and (2)). The relative frequency of each impactor trajectory is also defined as described in section II (i.e., Figure 7) and allows us to compute the probability that a random impact threat would approach the Earth with a given impact velocity v_{impact}. The asteroid size that yields a specific impact event depends then on the v_{impact} of the asteroid. The range of asteroid sizes that can possibly yield a given impact event (i.e., energy) can be estimated by considering the maximum and minimum bound of possible v_{impact} from the grid (see Table 1). A spherical shape and average density (i.e., 2600 g/m^3 [28]) have been assumed here. The relative frequency on which the different asteroid sizes (or masses M_{Ast} if spherical shape and average density is assumed) occur can be well modeled by a power law distribution [29]. A four-slope power law distribution is used, matching previous estimations [29] above and below 1-km and 10-m objects respectively, while showing a drop of a factor of 2/3 on the cumulative number of objects at 100-m diameter, as indicated by most recent studies on asteroid size-population [30]. The combination of relative frequency of the different v_{impact} and asteroid sizes allows us to estimate the expected frequencies for different impact events, as shown in Table 1.

A. Planetary protection of previously detected Earth-impacting objects

The aim of this section is to compute the probability to deflect a randomly generated impact threat in each one of the categories presented in Table 1, by the small kinetic impactor. This probability can also be understood as the fraction of impact risk within an impact event category that is safely removed by the deflection system. This probability, or fraction, not only depends on the size of our deflection system, in this case fixed to a 1-tonne kinetic impactor at Earth departure, but also on the available warning time $\Delta t_{warning}$, since this define how early in advance the asteroid can be pushed away from its collisional trajectory. Unfortunately, each different warning time $\Delta t_{warning}$ analyzed requires a full set of trajectory optimizations to each one of the 17,518 impacting ephemeris, and the latter requires a total of 100 days of computational time on a Intel Nehalem X5570 2.93 GHz machine. Thus, only a small set of five different warning times (i.e., 20, 15, 10, 5 and 2.5 years) was considered in order to offer a good compromise of computational cost, while offering still a satisfactory assessment of the influence of the warning time on the deflection capability of the kinetic impactor.

For each warning time $\Delta t_{warning}$, a full set of impacting trajectory optimizations that maximize the product $m_d \cdot \Delta \mathbf{v}_{S/C}\left(t_d\right)$, which ensures that maximum deflection, is computed. Since the set of optimal impact relative velocity $\Delta \mathbf{v}_{S/C}$, impact mass m_d and impact time t_d are known, the asteroid deflection distance Eq. (15) can now be redefined as a function of the parameter M_{Ast}. Thus, a threshold asteroid mass M_{Ast} can be found that matches

the minimum deflection distance required for the asteroid to miss the Earth. Since the virtual impactors are defined as objects with zero MOID, the minimum deflection to achieve a safe distance is equal to $\mathrm{MOID}_{\oplus}$ as in Eq. (5) (here not defined as an actual MOID of the asteroid but just as a distance for that particular passage.).

Equivalently, the maximum impact energy E_{impact} that can be deflected from each impacting trajectory can be computed by multiplying maximum deflected mass of each node by $0.5 \cdot v\left(a,e,i\right)_{impact}^{2}$. Figure 14 represents, by means of several slice cuts through the grid of results, the maximum impact energy that can be deflected by the proposed kinetic deflector if 20 years of warning time are available. As shown by Figure 14, the kinetic impactor achieves maximum deflection of 29,000 MT of energy, which is well into the global threat level. This of course does not mean that a 1 tonne-kinetic impactor is an efficient system against global impact events, since the maximum occurs for very high semi-major axis, high eccentricity and high inclination objects, i.e., regions on which the impact frequency is actually negligible. It is also interesting to note that the deflection efficiency increases the furthest away from (a=1, e=0, i=0^{o}), i.e., Earth-like orbits, despite the fact that transfer cost are higher and thus m_d decreases.

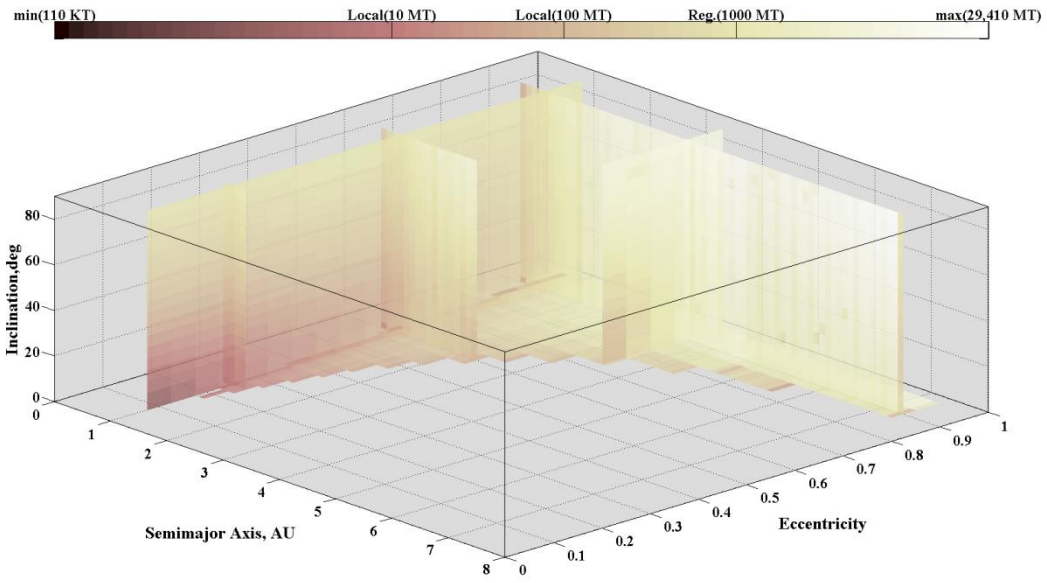

Figure 14: Maximum deflection capability of a 1-tonne kinetic impactor with 20 years of warning time as a function of {*a*,*e*,*i*}.

Let us see, with an example, a more detailed account of the information available at each node of the grid and for each warning time. As shown in Figure 7, each individual impacting ephemeris has allocated a normalized probability of occurrence, for example, the node corresponding to (a=0.95, e=0.175, i=2.5^{o}) has a relative probability of 5.8x10^{-4}, which is the result of integrating $f_I\left(a,e,i\right) = \rho \cdot g$, where ρ is the NEO density

distribution and g the collisional probability, from within the volume Δa=±0.05, Δe=±0.025 and Δi=±2.5 ^{o}. Note that an impacting trajectory such as that of Apophis [31] (i.e., (a=0.9223,e=0.191,i=3.3^{o})) would be included on the analysis as belonging to this node. The impact velocity v_{impact} associated with this node, as a result of Eq. (1) and (2), is 12.3 km/s. Each node has now also allocated a maximum deflected mass for each of the two impacting trajectories associated with each node (see Figure 2), which are the result of the previously described global trajectory optimization. In this example, the set of maximum deflected masses are: [2.8x10^{8} kg, 2.7x10^{8} kg], [2.2x10^{8} kg, 2.7x10^{8} kg], [1.6x10^{8} kg, 1.8x10^{8} kg], [5x10^{7} kg, 6x10^{7} kg] and [2.7x10^{7} kg, 3.8x10^{7} kg], which correspond to the 20, 15, 10, 5 and 2.5 years warning time. Thus, the maximum deflected energy corresponds to [5.06, 4.9], [3.9 4.9], [2.9 3.2], [0.9 1.1] and [0.4 0.7] MT.

For each individual node, we can compute the relative frequency of the different impact events by means of the asteroid size distribution discussed earlier. Since, given a node, the set of Keplerian parameters (a,e,i) is defined, and thus also v_{impact}, assuming spherical shape and an asteroid average density of 2,600 kg/m^{3} [28], one can compute impact event cumulative distribution as:

$$I_{eventD} = \frac{N(> D_{Elowbound}) - N(> D)}{N(> D_{Elowbound}) - N(> D_{Eupperbound})}, \tag{24}$$

where $N(>D)$ is the number of objects with diameter larger than diameter D, computed by means of the, previously mentioned, four-slope power law distribution function [30], and $D_{Elowbound}$ and $D_{Eupperbound}$ is the asteroid diameter that yields the minimum energy and maximum energy of a given impact category, respectively. Figure 15 shows impact event cumulative distribution for the node (a=0.95, e=0.175, i=2.5^{o}). See in the figure that, for example, a maximum deflection capability of 5 MT allows deflection of 88% of impacts in the Airburst category, while, of course, no protection is achieved in any other category.

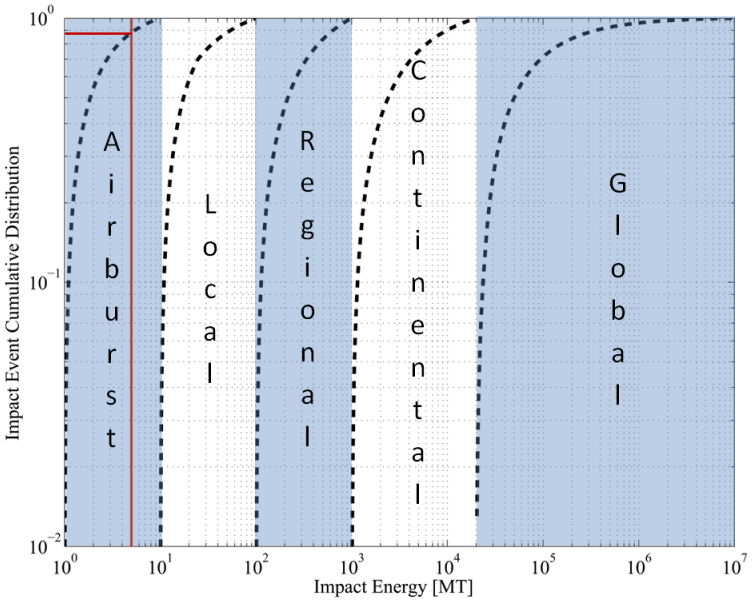

Figure 15: Impact event cumulative distribution for the node at (*a*=0.95, *e*=0.175, *i*=2.5°).

Thus the planetary protection achieved by the 1-tonne kinetic impactor at the (*a*=0.95, *e*=0.175, *i*=2.5°) node is [88.4%, 87.7%], [81.7%, 87.7%], [71.5%, 75.3%], [0% 9%] and [0% 0%] for 20, 15, 10, 5 and 2.5 years warning time, respectively, at airburst level. This result can be repeated for each node and each warning time and, finally, a weighted sum of all the nodes yields the final value of the planetary protection for a given warning time scenario. Note that the weights used are the relative impact frequencies at each node, i.e., half of the impact frequency of the node for each the two nodal impact ephemeris. The results of this procedure for each warning time are summarized in Table 2.

Table 2: Planetary Protection.

Type of event	Warning time				
	20 year	**15 years**	**10 years**	**5 years**	**2.5 years**
Airburst	99.4%	99.0%	98.1%	88.8%	26.9%
Local Damage	92.5%	88.3%	80.7%	51.4%	9%
Regional Damage	43.0%	31.7%	22.8%	9.5%	0.6%
Continental Damage	3.9%	1.8%	0.6%	0.03%	0%
Global Damage	0%	0%	0%	0%	0%

Interestingly, the results shown in Table 2, are much better than those computed on the "Apophis" node described in the previous paragraph. Note that Apophis asteroid [32], which represents an impact threat of order 500 MT due to its large size, thus a regional impact threat event, could not be deflected by the kinetic system proposed here, nevertheless the system could actually feasibly deflect similar threats on a 43% of the cases if 20

years of warning time were available. This result underlines the significance of the statistical analysis carried out on this paper, in order to obtain an unbiased measure of the efficiency of a deflection system.

Hence, while for a test-case so commonly used as Apophis, a 1-tonne kinetic impactor would prove rather insufficient as an impact mitigation measure, the results shown in Table 2 indicate a good impact hazard mitigation capability, if we take into account the simplicity of the strategy and the size of the deflection system. It is important to note that the planetary protection capabilities shown in Table 2 can be considered as being at the state-of-the-art of the current technology, or not far from it, by considering Deep Impact mission, a 973 kg Kinetic Impact scientific mission [33], as a technology demonstrator of the concept proposed here. Clearly, such a deflection system does not constitute a robust deflection system as the likelihood of deflecting large impact events is small even for long warning times. Nevertheless, if we consider the impact risk shown by Shapiro et al.[4], where it is seen that small objects, up to a 100 meters, constitute an important fraction of the impact risk (e.g., see figure 2.7 in [4]), we could then argue that a 1-tonne impact deflection system could defend against a very important fraction of the total impact risk.

B. Planetary protection with detection model

The planetary protection discussed so far assumes that any threatening object smaller than the maximum deflected size at the node could be deflected by the 1-tonne kinetic deflection system. This is therefore overlooking the possibility, as shown by Figure 13, that small objects may not be detectable and therefore the kinetic impactor may not be able to deflect them. While the results in Table 2 are particularly useful to measure the crude impact hazard mitigation efficiency of a small kinetic impactor, it is interesting to attempt a more realistic figure of planetary protection by considering the detection of threatening objects prior to the launch of the deflection system.

This new impact scenario assumes then that no threatening object is known 25 years prior to the impact date. A survey program is then started 25 years prior to the preset impact of the virtual threatening object and runs all the way to the impact time, detecting any object that meets the criteria described in section III.B. In such a scenario, only the impact threat posed by discovered objects can actually be mitigated by the kinetic impactor. Table 3 then shows the fraction of discovered threat within each of the impact categories described in Table 1. The fraction of discovered threats is, of course, increasing with an increasing survey time-span Δt_{survey} or a decreasing warning time $\Delta t_{warning}$. Recall, as defined section III.B, that the asteroid survey is assumed to run within times $[t_{\text{impact}}-25 \text{ years}, t_{\text{impact}}-\Delta t_{\text{warning}}]$. Note then that while a warning time of 20 years implies a 5 year

survey, a warning time of 5 year implies a much longer 20 years survey. Table 3 shows that small objects, of order a few tens of meter diameter, can easily escape detection, and thus the risk of undetected airburst and local damage events remains high even for long survey campaigns. On the other hand, larger impact energy events, such as events with continental and global consequences, are easily detectable with still long warning times for deflection. The regional impact event, e.g., Apophis threat, tends also to be discovered with certain ease, although the survey campaign requires a time-span longer than a decade to reach a high completion of discovered threat.

Table 3: Fraction of the impact threat discovered with the corresponding warning time. Hence, with 5, 10, 15, 20 or 22.5 years of survey time.

Type of event	Warning time/Survey time-span				
	20/5 year	**15/10 years**	**10/15 years**	**5/20 years**	**2.5/22.5 years**
Airburst	11.2%	20.8%	27.5%	34%	35.1%
Local Damage	19.3%	35.6%	47.8%	55.9%	62.6%
Regional Damage	41.4%	64.1%	73.6%	84.7%	92.7%
Continental Damage	81	92.9%	98.8%	99.6%	99.8%
Global Damage	98.7%	99.8%	100%	100%	100%

Despite the fact that Table 2 demonstrated a very high efficiency at deflecting low energy impact threats, the kinetic impactor may not be capable of deflecting a large portion of the impact risk on categories where many objects posing risk remain undiscovered or are discovered very late. We can then compute a new set of planetary protection, but this time also taking into account the minimum object size discovered at each node. Thus, the mitigated impact risk at each node is computed as:

$$I_{mitigated} = \frac{N(> D_{Minsize}) - N(> D_{Maxsize})}{N(> D_{Elowbound}) - N(> D_{Eupperbound})}, \tag{25}$$

where $D_{Minsize}$ is the minimum asteroid size that can be discovered at the node (as long as is not smaller than $D_{Elowbound}$) and $D_{Maxsize}$ is the largest asteroid size that can be deflected (as long as is not larger than $D_{Eupperbound}$).

In this scenario, we will also assume that the spacecraft is launched as early as the threat is discovered. Hence, for example, the kinetic impactor will be launched with 20 years warning time to attempt deflection of all impact threats discovered within the 5 first years of survey. Instead, the 15-years launch window is used to attempt deflection of any newly discovered threat during the previous 5 years of survey, and so on for the remaining warning time computed. This is equivalent to integrate the planetary protection as the survey duration advances and the warning time to deflect the asteroid decreases. Note that, ideally, we would like to integrate this for a continuous change of warning time and survey time, but this would require a full set of trajectory

optimizations for each warning time. Due to the computational cost of these, we proceed with a discreet set of warning times, which is believed to provide a good estimation of the figure intended. Table 4 summarizes the cumulative planetary protection as the survey time increases.

Table 4: Planetary Protection on the detection-required scenario.

Type of event	Warning time/Survey time-span				
	20/5 year	**15/10 years**	**10/15 years**	**5/20 years**	**2.5/22.5 years**
Airburst	10.8%	20.4%	26.4%	32.3%	32.7%
Local Damage	15.8%	29.8%	38.6%	42.9%	43.1%
Regional Damage	15.8%	23.4%	25.9%	27.1%	27.1%
Continental Damage	2%	2.5%	2.6%	2.6%	2.6%
Global Damage	0%	0%	0%	0%	0%

The results shown in Table 4 demonstrate again a very good efficiency of a 1-tonne kinetic impactor on the low range of impact energies (1 to 100 MT). The issue this time, and as shown by Table 3, is that the undiscovered impact threat within these energies poses a limit threshold on the feasible hazard mitigation. On the other hand, higher energy events (>100 MT) are more efficiently discovered. However, the 1-tonne kinetic impactor analyzed in this paper is not capable of providing a reliable mitigation against such large impact threats. It is nevertheless very remarkable the planetary protection achieved on the regional and continental impact categories, considering the small size of the deflection system. Note that the threat posed by Apophis lies on the Regional damage category and thus the results here show that a 1-tonne kinetic impact mission could suffice to deflect 27% of equivalent impact threats.

It has been shown that while airburst and local impact threats could be very efficiently mitigated by a small kinetic impactor, as long as detection of these type of threats is granted, larger impact threat (>100 MT) cannot be efficiently mitigated by a small deflection system. The question that arises then is how large a kinetic impactor system should be in order to provide a considerable planetary protection on impact threats above 100 MT of energy. Figure 16 shows the evolution of the cumulative planetary protection with warning time from 20 to 2.5 years and survey duration varying accordingly from 5 to 22.5 years (i.e., equivalent to the column 2.5/22.5 years in Table 4) as a function of the launched wet mass of the system. Note that the final asteroid deflection is proportional to the launched mass, through the rocket's equation to compute the impacting mass and Eq. (15) to compute the deflection, and thus the optimizations presented throughout the paper can be reused with a varying launch mass in order to compute the planetary protection level of differently sized kinetic impactors.

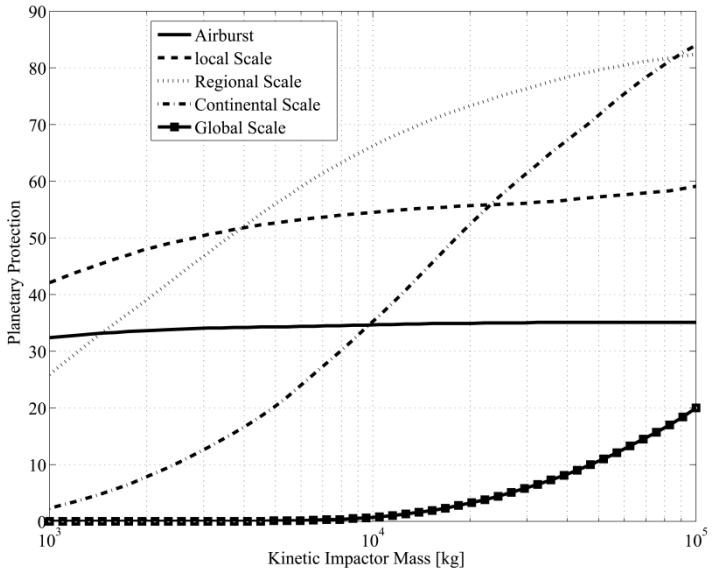

Figure 16: Evolution of cumulative planetary protection for 20 to 2.5 years warning time as a function of the kinetic impactor mass at launch.

Figure 16 shows how the planetary protection increases for all impact events as the kinetic impactor mass increases. At first glance, the planetary protections for the five types of impact events seem to behave very differently, but in reality all of them increase to the limiting point of mitigating all discovered risk. As summarized in Table 3, the kinetic impactor can only defend against impact threats coming from the discovered population of impactors (e.g., 35.1% of airburst, 62.6% of local events, etc), and thus this sets a hard limit on the planetary protection that can be achieved. On the other hand, all curves of planetary protection undergo an important increase that occurs when impactor size is large enough to protect against the impacting trajectories with highest impact relative frequency (see Figure 7).

Some final remarks on the accuracy of the results shown throughout the paper are in order. The planetary protection shown here should be taken as a rough quantitative estimate of the merit of the kinetic impactor as an impact mitigation system. However, the estimates are likely to be conservative. The interception transfer trajectories, for example, have been computed as a simple Lambert's arc transfer. A more comprehensive optimization of the interception transfer could include multiple planetary fly-byes, which would certainly increase the efficiencies computed here [34]. Also the enhancement factor β in Eq.(15) has been conservatively chosen [14]. Both an increase of the impact velocity, due to improved interception trajectories, or an increase on the β factor could potentially increase the momentum transfer efficiency of the impact, Eq. (15), by a factor of several units, which would consequently increase the planetary protection as if the kinetic impactor mass would have increased by the same factor. The other factors intervening in the calculation of the planetary protection

(e.g., impact probability, NEO model, deflection formulas) are estimated to be accurate enough so that possible error models would contribute with very small changes, on the order of small percents, on the planetary protection. The only exception perhaps is the detection model described in Section III.C. Despite being only a rough estimate of the detection capabilities of an asteroid survey, the detection model should have a relatively small influence on the general significance of the results shown in Section IV.B. Nevertheless, the discovery statistics provided by the model used here seem a reasonable estimate also when compare to more complex survey systems [25].

IV. Conclusions

The paper presented a novel approach to measure the efficiency of a deflection system based on a statistical analysis of a very large sample of impacting ephemerides. The figure of merit used to measure the deflection efficiency, named as Planetary Protection of the deflection system, is an attempt to obtain a measure not directly related with the orbital elements of the impacting object. A realistic set of impact threat scenarios is built by generating more than 17,000 virtual Earth-impacting trajectories with orbital elements homogeneously distributed and the relative frequency of each of these Earth-impacting orbits is estimated.

For each single virtual threatening asteroid's orbit, the interception trajectory launching from Earth is optimized to maximize the displacement of the asteroid at the minimum orbital intersection distance following the kinetic deflection. Two distinct cases are analyzed; in the first one the threatening object is assumed to be known at the beginning of the launch window. In a second scenario, instead, the threatening asteroid is assumed to be unknown, thus needs to be discovered through survey during the available launch window. The planetary protection index is defined as the fraction of impact hazard (over all the possible hazard scenarios) that a deflection system would be able to mitigate. By means of the estimation of the planetary protection provided by a 1-tonne kinetic impactor the paper demonstrated a very good efficiency at impact hazard mitigation of such a high technology-readiness level deflection system. Thus, it is argued that such a system is a good example of current deflection capabilities, as suggested by past missions such as Deep Impact.

V. Acknowledgments

The authors would like to thank Prof. Colin McInnes, director of the Advanced Space Concepts Laboratory for the support and careful read of the paper, and Dr. Massimiliano Vasile for the valuable discussions on the trajectory results. We thank William Bottke for kindly providing us with the NEA distribution data. The

simulations were performed on the Faculty of Engineering High Performance Computer facility, University of Strathclyde. The work was supported by the European Research Council grant 227571 (VISIONSPACE).

VI. References

[1] Chapman, C. R., "The Hazard of near-Earth Asteroid Impacts on Earth," *Earth and Planetary Science Letters*, Vol. 2, No. 1, 2004, pp. 1-15. doi: 10.1016/j.epsl.2004.03.004

[2] Alvarez, L. W., Alvarez, W., Asaro, F. and Michel, H. V., "Extraterrestrial Cause for the Cretaceous-Tertiary Extinction," *Science*, Vol. 208, No. 4448, 1980, pp. 1095-1108. doi: 10.1126/science.208.4448.1095

[3] Steel, D., "Tunguska at 100," *Nature*, Vol. 453, 2008, pp. 1157-1159. doi: 10.1038/4531157a

[4] Shapiro, I. I., A'Hearn, M., Vilas, F. and Et.al., "Defending Planet Earth: Near-Earth Object Surveys and Hazard Mitigation Strategies," National Research Council, 2010.

[5] Joseph, N. S., "Asteroid Hazard Mitigation Using the Yarkovsky Effect," *Science*, Vol. 296, No. 5565, 2002, pp. 77-77. doi: 10.1126/science.1069577

[6] Kleiman, L. A., *Project Icarus: An Mit Student Project in Systems Engineering*, The MIT Press, Cambridge, Massachusetts, 1968.

[7] Scheeres, D. J. and Schweickart, R. L., "The Mechanics of Moving Asteroids," *Proceedings of the Planetary Defense Conference*, American Institute of Aeronautics and Astronautics, Orange County, California, 2004. doi: Paper AIAA-2004-1446

[8] Edward, T. L. and Stanley, G. L., "Gravitational Tractor for Towing Asteroids," *Nature*, Vol. 438, 2005, pp. 177-178. doi: 10.1038/438177a

[9] J.Olds, A.Charania and M.G.Schaffer, "Multiple Mass Drivers as an Option for Asteroid Deflection Missions," *Proceedings of the Planetary Defense Conference*, edited by A. American Institute of and Astronautics.

[10] Vasile, M., "A Multimirror Solution for the Deflection of Dangerous Neos," *Communications in Nonlinear Science and Numerical Simulation*, Vol. 14, 2008, pp. 4139-4152.

[11] Bombardelli, C. and Peláez, J., "Ion Beam Shepherd for Asteroid Deflection," *Journal of Guidance Control Dynamics*, Vol. 34, No. 4, 2011, pp. 1270-1272. doi: 10.2514/1.51640

[12] Sanchez, J. P., Colombo, C., Vasile, M. and Radice, G., "Multi-Criteria Comparison among Several Mitigation Strategies for Dangerous near Earth Objects," *Journal of Guidance, Control and Dynamics*, Vol. 32, No. 1, 2009, pp. 121-142. doi: 10.2514/1.36774

[13] Ahrens, T. J. and Harris, A. W., "Deflection and Fragmentation of near-Earth Asteroids," *Nature*, Vol. 360, 1992, pp. 429-433. doi: 10.1038/360429a0

[14] Wolters, S. D., Ball, A. J., Wells, N., Saunders, C. and McBride, N., "Measurement Requirements for a near-Earth Asteroid Impact Mitigation Demonstration Mission," *Planetary and Space Science*, Vol. 59, No. 13, 2011, pp. 1506-1515. doi: 10.1016/j.pss.2011.06.015

[15] "Near-Earth Objects Survey and Deflection Analysis of Alternatives," National Aeronautics and Space Administration, 2007.

[16] Schaffer, M. G., Charania, A. C. and Olds, J. R., "Evaluating the Effectiveness of Different Neo Mitigation Options," *2007 Planetary Defense Conference*, edited by American Institute of Aeronautics, Washington, D.C., 2007.

[17] Vasile, M. and Colombo, C., "Optimal Impact Strategies for Asteroid Deflection," *Journal of Guidance, Control, and Dynamics*, Vol. 31, No. 4, 2008, pp. 858-872. doi: 10.2514/1.33432

[18] Bottke, W. F., Morbidelli, A., Jedicke, R., Petit, J.-M., Levison, H. F., Michel, P. and Metcalfe, T. S., "Debiased Orbital and Absolute Magnitude Distribution of the near-Earth Objects," *Icarus*, Vol. 156, No. 2, 2002, pp. 399-433. doi: 10.1006/icar.2001.6788

[19] Opik, E. J., "Collision Probabilities with the Planets and the Distribution of Interplanetary Matter," *Proceedings of the Royal Irish Academy. Section A: Mathematical and Physical Sciences*, Vol. 54, 1951, pp. 165-199

[20] Rayman, M. D., Fraschetti, T. C., Raymond, C. A. and Russell, C. T., "Dawn: A Mission in Development for Exploration of Main Belt Asteroids Vesta and Ceres," *Acta Astronautica*, Vol. 58, 2006, pp. 605-616. doi: 10.1016/j.actaastro.2006.01.014

[21] A'Hearn, M. F., Belton, M. J. S., Delamere, W. A., Kissel, J., Klaasen, K. P., McFadden, L. A., Meech, K. J., Melosh, H. J., Schultz, P. H., Sunshine, J. M., Thomas, P. C., Veverka, J., Yeomans, D. K., Baca, M. W., Busko, I., Crockett, C. J., Collins, S. M., Desnoyer, M., Eberhardy, C. A., Ernst, C. M., Farnham, T. L., Feaga, L., Groussin, O., Hampton, D., Ipatov, S. I., Li, J.-Y., Lindler, D., Lisse, C. M.,

Mastrodemos, N., Owen, W. M., Richardson, J. E., Wellnitz, D. D. and White, R. L., "Deep Impact: Excavating Comet Tempel 1," *Science*, Vol. 310, No. 5746, 2005, pp. 258-264. doi: 10.1126/science.1118923

[22] Sanchez, J. P. and McInnes, C. R., "Asteroid Resource Map for near-Earth Space," *Journal of Spacecraft and Rockets*, Vol. 48, No. 1, 2011, pp. 153-165. doi: 10.2514/1.49851

[23] Vasile, M., "A Behavioral-Based Meta-Heuristic for Robust Global Trajectory Optimization," *Proceedings of the IEEE Congress on Evolutionary Computation (CEC 2007)*, Inst. of Electrical and Electronics Engineers, Piscataway, NJ, 2007, pp. 2056–2063.

[24] Vasile, M. and Locatelli, M., "A Hybrid Multiagent Approach for Global Trajectory Optimization," *Journal of Global Optimization*, Vol. 44, No. 4, 2009, pp. 461–479. doi: 10.1007/s10898-008-9329-3

[25] Veres, P., Jedicke, R., Wainscoat, R., Granvik, M., Chesley, S., Abe, S., Denneau, L. and Grav, T., "Detection of Earth-Impacting Asteroids with the Next Generation All-Sky Surveys," *Icarus*, Vol. 203, No. 2, 2009, pp. 472-485. doi: 10.1016/j.icarus.2009.05.010

[26] Bowell, E., Hapke, B., Domingue, D., Lumme, K., Peltoniemi, J. and Harris, A. W., *Asteroids Ii*, Univ. of Arizona Press, Tucson, 1989, pp. 524–556.

[27] Stuart, J. S., "Observational Constraints on the Number, Albedos, Size, and Impact Hazards of the near-Earth Asteroids," Massachusetts Institute of Technology, 2003.

[28] Chesley, S. R., Chodas, P. W., Milani, A. and Yeomans, D. K., "Quantifying the Risk Posed by Potential Earth Impacts," *Icarus*, Vol. 159, No. 2, 2002, pp. 423-432. doi: 10.1006/icar.2002.6910

[29] Stokes, G. H., Yeomans, D. K., Bottke, W. F., Chesley, S. R., Evans, J. B., Gold, R. E., Harris, A. W., Jewitt, D., Kelso, T. S., McMillan, R. S., Spahr, T. B. and Worden, P., "Study to Determine the Feasibility of Extending the Search for near-Earth Objects to Smaller Limiting Diameters," NASA, 2003.

[30] Harris, A. W., "An Update of the Population of Neas and Impact Risk," *Bulletin of the American Astronomical Society*, Vol. 39, 2007, p. 511. doi: 2007DPS....39.5001H

[31] Chesley, S. R., "Potential Impact Detection for near-Earth Asteroids: The Case of 99942 Apophis (2004 Mn 4)," *Proceedings of the Asteroids, Comets and Meteors*, edited by D.Lazzaro, S.F. Mello, and J.A.Fern ndez, Vol. 229, International Astronomical Union, 2005. doi: 10.1017/s1743921305006769

[32] M.Delbo, A.Cellino and E.F.Tedesco, "Albedo and Size Determination of Potentially Hazardous Asteroids:(99942) Apophis," *Icarus*, Vol. 188, 2007, pp. 266-269. doi: 10.1016/j.icarus.2006.12.024

[33] Wissler, S., Rocca, J. and Kubitscheck, D., "Deep Impact Comet Encounter: Design, Development and Operations of the Big Event at Tempel 1," *Proceedings of the Space System Engineering Conference* Atlanta, 2005.

[34] Anastassios, E. P., Theresa, D. K., MatthewA.Vavrina, DanielW.Parcher, Paul, A. F., Gregory, J. W. and Jon, A. S., "1stact Global Trajectory Optimisation Competition: Results Found at the Jet Propulsion Laboratory," *Acta Astronautica*, Vol. 61, No. 9, 2007, pp. 806-815. doi: 10.1016/j.actaastro.2007.03.013